Small Science

small science Open Access
www.small-science-journal.com

RESEARCH ARTICLE OPEN ACCESS

Piperine Nanoparticles Significantly Improved Fragile X–Associated Tremor/Ataxia Syndrome via Mitigating RNA and Repeat-Associated Non-AUG Toxicities

Jiahao Li[1] | Mingxi Ou[2] | Zhefan Stephen Chen[2,3] | Weikang Ban[1] | Ho Yin Edwin Chan[2,3] | Sharon Shui Yee Leung[1] | Zhong Zuo[1]

[1]Guangdong-Hong Kong-Macao Joint Laboratory for New Drug Screening, School of Pharmacy, Faculty of Medicine, The Chinese University of Hong Kong, Shatin, Hong Kong SAR | [2]School of Life Sciences, Faculty of Science, The Chinese University of Hong Kong, Shatin, Hong Kong SAR | [3]Gerald Choa Neuroscience Institute, The Chinese University of Hong Kong, Shatin, Hong Kong SAR

Correspondence: Zhong Zuo (joanzuo@cuhk.edu.hk)

Received: 27 July 2026 | **Revised:** 29 October 2026 | **Accepted:** 31 October 2026

Keywords: CGG repeat *Drosophila* | CGG repeat mice | FXTAS | piperine nanoparticles

ABSTRACT

Fragile X–associated tremor/ataxia syndrome (FXTAS) is a neurodegenerative disorder driven by fragile X messenger ribonucleoprotein 1 (*FMR1*) premutation CGG repeats on the X chromosome, causing RNA and repeat-associated non-AUG (RAN) toxicities. Although piperine demonstrated preliminary mitigation of RNA toxicity, its poor aqueous solubility restricted further development. The current study evaluated piperine nanoparticles (PIP NPs) with enhanced solubility for FXTAS management. Briefly, PIP NPs were prepared using flash nanoprecipitation followed by assessing their impact on both CGG repeat *Drosophila* and mouse models. PIP NPs could significantly ameliorate the climbing deficits, protect against early-stage mortality (100 μM) and preserve retinal integrity in CGG repeat *Drosophila*, and rescue motor coordination and abnormal learning conditioning in CGG repeat mice, while reducing toxic *FMR1* mRNA, restoring *Drosophila* fragile X messenger ribonucleoprotein 1 (dFmr1) or fragile X messenger ribonucleoprotein (FMRP) expression, suppressing FMRpolyG-GFP production in *Drosophila*, and mitigating ubiquitin-positive intranuclear inclusions. Based on the findings, molecular docking analyses were adopted to provide a computational structural rationale for the proposed interactions between piperine and DExH-box helicase 9 (DHX9)/death-associated protein 5 (DAP5)/heat shock protein 70 (Hsp70). The serial in vitro, in vivo, and in silico investigations consistently demonstrated PIP NPs as a promising therapeutic candidate for FXTAS.

1 | Introduction

Fragile X–associated tremor/ataxia syndrome (FXTAS) affects approximately 1 in 8000 men over 50 years of age and presents with progressive action tremor, gait ataxia, and cognitive decline, including executive dysfunction and memory impairment [1, 2]. FXTAS is generally considered to be caused by a CGG repeat expansion in the fragile X messenger ribonucleoprotein 1 (*FMR1*) gene on the X chromosome. In healthy individuals, the *FMR1* gene contains fewer than 45 CGG triplets, whereas in FXTAS patients, this gene has 55–200 CGG triplet repeats [3]. Unlike full mutation fragile X syndrome (>200 CGG repeats), premutation alleles typically lead to elevated *FMR1* mRNA level with normal to moderately reduced levels of the *FMR1* protein (FMRP) due to translational inefficiency, a crucial RNA-binding protein implicated in diverse biological processes such as neuronal plasticity and the regulation of neuronal networks [3]. FXTAS can be explained by three primary molecular mechanisms. First, the formation of R-loops during the expansion of CGG triplet repeats at the *FMR1* locus increases susceptibility to DNA damage.

This is an open access article under the terms of the Creative Commons Attribution License, which permits use, distribution and reproduction in any medium, provided the original work is properly cited.

© 2026 The Author(s). *Small Science* published by Wiley-VCH GmbH.

Second, the repeat-associated non-AUG (RAN) translation of expanded CGG repeats produces deleterious proteins, such as the FMRpolyG peptide. Third, the expanded *FMR1* premutation mRNA sequesters essential RNA-binding proteins, which, along with RAN translation products, generate ubiquitin-positive intranuclear inclusions within the brain, which contribute to neurodegeneration [3, 4]. Consequently, a multitarget strategy that reduces *FMR1* transcript abundance, suppresses RAN translation, and clears out ubiquitin-positive intranuclear inclusions offers a promising approach to mitigate the disease comprehensively.

Currently available medications can only alleviate the symptoms of FXTAS [2, 5], and no treatment is available to halt its progression. Recent studies have demonstrated that small-molecule compounds can be used to neutralize CGG expansion toxicity [6–13]. Among these compounds, piperine directly binds r(CGG)n with selectivity and reduces toxic peptide production in cells [12]. Furthermore, piperine exhibited high permeability across the blood–brain barrier, suggesting its potential for effective central nervous system (CNS) permeation [14]. However, its low aqueous solubility (0.04 mg/mL) [15] has limited its further development as a therapeutic agent. We previously developed a piperine nanoparticles (PIP NPs) with markedly enhanced aqueous solubility to 50 mg/mL and 5 times higher brain exposure after oral administration compared with the piperine suspension [16], thereby enabling the further evaluation of its effects in FXTAS animal models.

Currently, animal models, including *Drosophila* and mouse models of FXTAS, serve as valuable tools for replicating the features of FXTAS, aiding drug development efforts [17]. The CGG repeat *Drosophila* FXTAS model exhibits retinal degeneration when mutant CGG repeat RNA is expressed in photoreceptor neurons [18]. Moreover, locomotor impairments [18] and reduced lifespan [19] have been documented in CGG repeat flies when CGG repeats are expressed throughout the nervous system. In addition, a CGG repeat mice model had been established, which exhibited abnormal learning and memory abilities, impaired motor coordination [20], and the formation of neuronal intranuclear inclusions [21]. These models, therefore, facilitate the screening and mechanistic studies of potential drug candidates for FXTAS treatment.

In this study, we evaluated the therapeutic efficacy of PIP NPs using CGG repeat *Drosophila* and mouse models by assessing behavioral and the pathological biomarker. Furthermore, molecular docking simulations were performed to explain the therapeutic efficacy of PIP NPs.

2 | Methodology

2.1 | Materials

Piperine (>97% purity) and Poloxamer 188 were sourced from Sigma–Aldrich Chemie GmbH (Germany) while Eudragit L100-55 was provided by Evonik Röhm GmbH (Darmstadt, Germany). Acetonitrile was purchased from RCI Labosan Ltd. (Bangkok, Thailand). HPLC-grade ethanol and methanol were obtained from DAEJUNG (Korea) and Merck (Germany), respectively. Deionized water was prepared using a Millipore purification system (Milford, MA, USA).

2.2 | PIP NPs

PIP NPs were prepared as previously reported [16] by flash nanoprecipitation using a four-stream multi-inlet vortex mixer. Vehicle nanoparticles (vehicle) were prepared identically without piperine. Briefly, to prepare PIP NPs, piperine (180 mg) and Eudragit L100-55 (600 mg) were dissolved in ethanol (24 mL) and rapidly mixed with poloxamer 188 (180 mg) water solution (67.2 mL) via syringe pumps (Model PHD 2000, Harvard Apparatus, MA, USA) under the flow rates of 6 and 16.8 mL/min, respectively. The resulting solution was concentrated under reduced pressure to reach the target concentration of piperine at around 3 mg/mL. The properties of the nanoparticles were characterized by measuring the particle size, polydispersity index (PDI), and zeta potential using a submicron particle size analyzer (DelsaNano C, Beckman Coulter, Osaka, Japan). The final concentration of piperine in the nanoparticles was quantified using a validated high-performance liquid chromatography (HPLC) with DAD detector as reported previously [16].

2.3 | Effect of PIP NPs on Behavior in CGG Repeat *Drosophila*

2.3.1 | Preparation of CGG Repeat Drosophila

2.3.1.1 | Lines. The *UAS-CGG$_{90}$-EGFP Drosophila* with a CyO balancer chromosome carrying Cyo markers [8, 18] was obtained from Professor Stephen Warren at Emory University, USA. w^{1118} (control), *elav-GAL4*, and *GMR-GAL4* flies were obtained from the Bloomington *Drosophila* Stock Center.

2.3.1.2 | Crosses. Virgin female *elav-GAL4* or *GMR-GAL4* flies were collected and crossed with male *UAS-EGFP-CGG$_{90}$* or w^{1118} flies. Only the first filial generation (F1) flies with straight wings were selected for the experiments.

2.3.1.3 | Diet and Dosing. Heated cornmeal medium (~10 mL/vial) was mixed with vehicle NPs or PIP NPs with an amount equivalent to 5, 50, or 100 μM piperine. Experiments for *elav > CGG$_{90}$* and *elav > w^{1118}* flies were conducted at 29 °C; while experiments for *GMR > CGG$_{90}$* and *GMR > w^{1118}* flies were conducted at 21.5 °C unless stated. The fly crossing, grouping, and assessment schedule are presented in Figure 1A.

2.3.1.4 | Verification of Climbing Ability in elav > CGG$_{90}$ Drosophila. To establish the CGG repeat model for evaluating climbing ability, parents of wild-type (WT, *elav > w^{1118}*) and transgenic (*elav > CGG$_{90}$*) flies were raised on cornmeal in an incubator at 25 °C. After 0 day posteclosion (dpe), F1 flies with straight wings were collected and transferred to an incubator at 29 °C. At 20 dpe, flies were anesthetized with carbon dioxide and placed in transparent 15 mL centrifuge tubes for at least 1 h to recover, followed by banging the flies to the bottom of the tubes. The total number of flies that failed to climb higher than the 2 cm mark on the tubes in 25 s was counted. Every trial was repeated three times with 5 min intervals. The climbing failure rate was calculated using the following equation. A significant difference in the climbing failure rate between control and *CGG$_{90}$* transgenic flies was considered to demonstrate the successful development of the model for testing climbing ability.

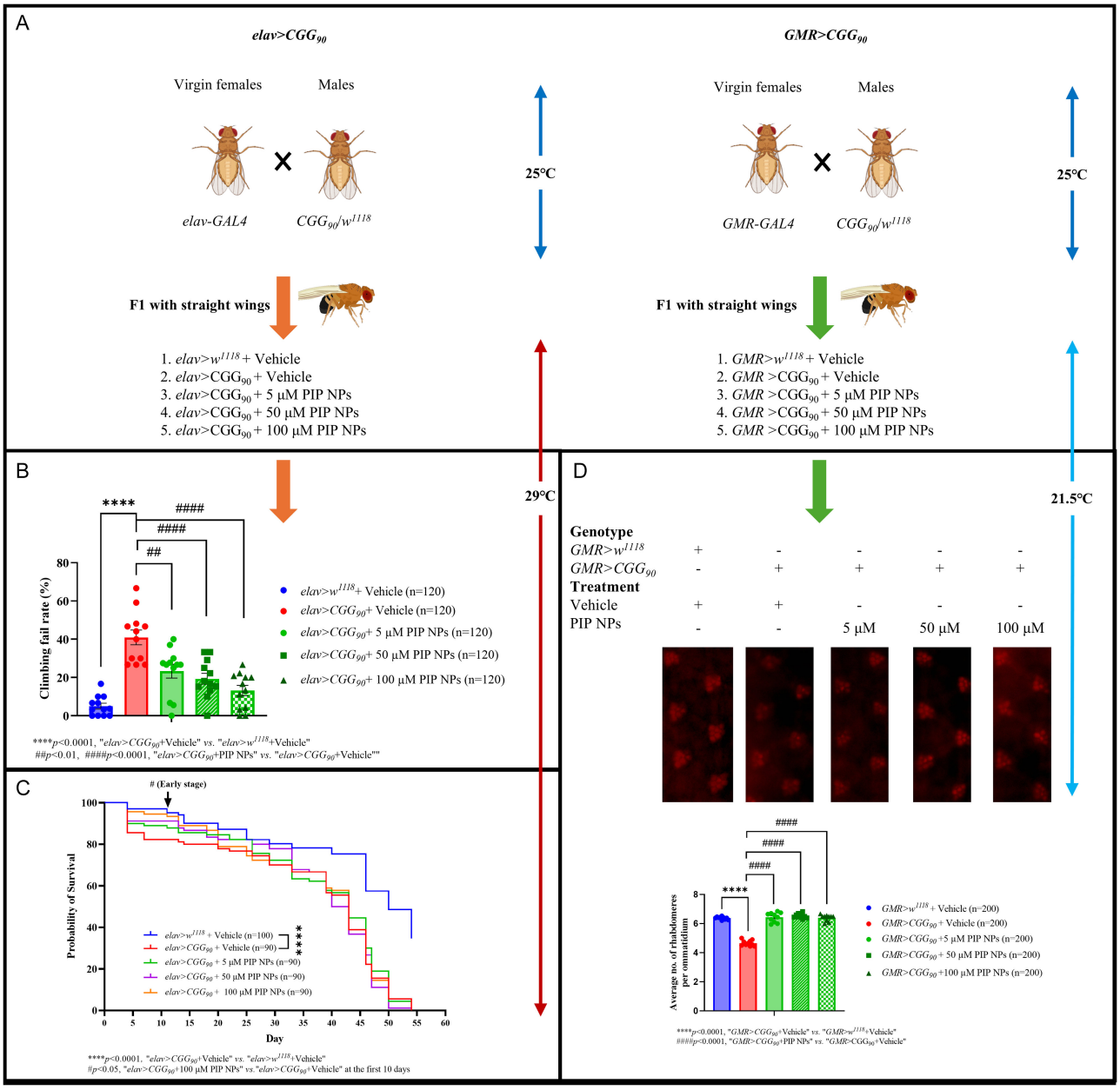

FIGURE 1 | Experimental design and therapeutic evaluation of PIP NPs in CGG repeat *Drosophila* models. (A) Schematic illustration of the crossing and grouping strategy for PIP NPs treatment at 5, 50, and 100 μM. (B) Climbing ability analysis ($n = 120$ per group from three independent crosses). (C) Lifespan assay ($n = 100$ for $elav > w^{1118}$, $n = 90$ per treatment group from three independent crosses) in $elav > CGG_{90}$ *Drosophila*. (D) Pseudopupil assay in $GMR > CGG_{90}$ *Drosophila* ($n = 200$ ommatidia from ten flies per group from three independent crosses). Data was presented as mean±SEM. Statistical significance was determined by Kaplan–Meier (C) or one-way ANOVA followed by Tukey's post hoc test (B, D). ****$p < 0.0001$; #$p < 0.05$, ##$p < 0.01$, and ####$p < 0.0001$.

$$\text{Climbing failure rate}\,(\%) = \frac{\text{Number of flies remaining at the bottom at 25 seconds } (< 2\text{ cm})}{\text{Total number of flies at 25 seconds}} \times 100\,\%$$

2.3.1.5 | *Verification of Lifespan in elav > CGG_{90} Drosophila.* To evaluate the effect of PIP NPs on lifespan, the growing environment was optimized for evaluating lifespan. The parents of wild-type ($elav > w^{1118}$) and transgenic ($elav > CGG_{90}$) flies were raised on cornmeal in an incubator at 25 °C. After 0 dpe, F1 flies with straight wings were collected for growing environment optimization by modifying the incubator temperature and food exchange frequency. A significant difference in lifespan between wild-type and transgenic flies was considered to indicate the successful optimization of the growing environment for lifespan evaluation.

2.3.1.6 | *Verification of Pseudopupil in $GMR > CGG_{90}$ Drosophila.* The effect of PIP NPs on retinal degeneration in $GMR > CGG_{90}$ *Drosophila* was evaluated by comparing the average number of rhabdomeres per ommatidium. To establish the CGG repeat model for pseudopupil evaluation, F1 flies ($GMR > w^{1118}$ and $GMR > CGG_{90}$) were raised on cornmeal in an incubator at 21.5 °C, and the average number of rhabdomeres per ommatidium was counted in 200 ommatidia from ten F1 flies at 30 dpe. The

eyes of individual flies were inspected using a stereomicroscope (CX31; Olympus, Japan). Ommatidium images were captured using a SPOT Insight CCD camera (Diagnostic Instruments, Sterling Heights, MI, USA), and subsequent image processing was conducted using the SPOT Advanced (Version 5.2; Diagnostic Instruments) and Photoshop 2020 (Adobe Systems, USA). A significant difference in the average number of rhabdomeres per ommatidium between wild-type and CGG repeat flies was considered to indicate the successful development of the model for retinal degeneration.

2.3.2 | PIP NPs Treatment and Behavior Assessments

As shown in Figure 1A (left panel), to evaluate the effect of PIP NPs on the climbing ability of CGG repeat *Drosophila*, one set of F1 flies with straight wings was used. F1 flies were randomly assigned to treatment groups. At 0 dpe, F1 of $elav > w^{1118}$ flies were fed cornmeal mixed with vehicle NPs ($n = 120$ from three independent crosses), whereas F1 of $elav > CGG_{90}$ flies were fed cornmeal mixed with vehicle NPs or PIP NPs at 5, 50, or 100 μM piperine ($n = 120$ per group from three independent crosses) in an incubator at 29 °C. At 20 dpe, the climbing failure rates of $elav > w^{1118}$ and $elav > CGG_{90}$ flies subjected to different treatments were obtained and compared. The heads of flies were collected after the climbing ability tests. No fewer than 100 heads were immediately frozen in liquid nitrogen and stored at −80 °C for subsequent mRNA and protein extraction, while no fewer than 3 heads from three independent crosses were immersed in ice-cold 4% paraformaldehyde for subsequent immunofluorescence experiments. Similarly, to evaluate the effect of PIP NPs on the lifespan of CGG repeat *Drosophila*, another set of F1 flies with straight wings was randomly assigned to treatment groups under optimized growing conditions. At 0 dpe, F1 $elav > w^{1118}$ flies were fed with cornmeal mixed with vehicle NPs ($n = 100$ from three independent crosses), whereas F1 $elav > CGG_{90}$ flies were fed with cornmeal mixed with vehicle NPs ($n = 90$ from three independent crosses) or PIP NPs at 5, 50, or 100 μM piperine ($n = 90$ per treatment group from three independent crosses). The number of deaths was counted twice a week. The lifespan of $elav > w^{1118}$ flies, vehicle-treated $elav > CGG_{90}$, and PIP NPs treated $elav > CGG_{90}$ flies was calculated and compared. In addition, to assess the potential impact of PIP NPs on $elav > w^{1118}$ flies, another set of experiments was conducted. Briefly, $elav > w^{1118}$ flies were treated with either vehicle NPs or 100 μM PIP NPs and maintained in an incubator at 29 °C. The climbing failure rates ($n = 100$ per group from three independent crosses) at 20 dpe and the survival rates ($n = 144$ per group from three independent crosses) at 30 dpe were recorded and compared.

As shown in Figure 1A (right panel), to evaluate the effect of PIP NPs on the retinal integrity of CGG repeat *Drosophila* using the pseudopupil assay, another set of F1 flies with straight wings was used. At 0 dpe, F1 of $GMR > w^{1118}$ flies was fed cornmeal mixed with vehicle NPs, whereas F1 of $GMR > CGG_{90}$ flies was fed cornmeal mixed with vehicle NPs or PIP NPs at 5, 50, or 100 μM piperine in an incubator at 21.5 °C. At 30 dpe, the average number of rhabdomeres per ommatidium was counted and compared between the $GMR > w^{1118}$ controls and the $GMR > CGG_{90}$ flies subjected to the different treatments ($n = 200$ ommatidia from ten flies per treatment group from three independent crosses), followed by collecting the heads of all flies for subsequent experiments. No fewer than 100 heads were immediately frozen in liquid nitrogen and stored at −80 °C for subsequent mRNA and protein extraction, while no fewer than 3 heads from three independent crosses were immersed in ice-cold 4% paraformaldehyde for subsequent immunofluorescence experiments.

2.3.3 | Evaluation of FMR1 mRNA, dFmr1, Canonical GFP, and Noncanonical FMRpolyG-GFP Protein Level and the Presence of UbiquitIn-Positive Intranuclear Inclusions

2.3.3.1 | *FMR1 mRNA Level Measurement.* To evaluate the effect of PIP NPs on the *FMR1* mRNA level in the CGG repeat *Drosophila*, *Drosophila* heads collected previously were subjected to total RNA extraction (10 heads per test, altogether 30 heads for three independent biological replicates) using an animal total RNA isolation kit (FOREGENE, Chengdu, China) according to the instructions from manufacturer. The total RNA was reverse-transcribed into cDNA using RT EasyII (FOREGENE, China). For quantitative analyses, reverse transcription–polymerase chain reaction (RT–qPCR) was conducted using RT–PCR Easy-SYBR Green I (FOREGENE, China) in the Light Cycler 480 II system (Roche, Switzerland) or Light Cycler PRO system (Roche, Switzerland) under the following thermal cycling conditions: initial denaturation and enzyme activation at 95 °C for 3 min (one cycle), followed by 40 cycles of denaturation at 95 °C for 10 s, annealing at 65 °C for 10 s, and extension at 72 °C for 20 s. Subsequently, melting curve analyses (one cycle) were performed after PCR to ensure the specificity of the amplified products.

Relative mRNA expression was normalized to internal control to standardize the data. The following primer sequences, reported previously [18, 22, 23], were used in the study. RPL18, the internal control primer for mRNA analyses, was selected based on its superior expression stability across all experimental groups.

CGG repeat-specific primers: GCTCAGCTCCGTTTCGGTTTCA CTTCCGGT (primer C); AGCCCCGCACTTCCACCACCAGC TCCTCCA (primer F).

GAPDH-1: GGTCCTTCGGGCAAACTG (F); CCTTAGCCTTGA TCTCATCGTA (R).

GAPDH-2: CCTGGCCAAGGTCATCAATG (F); ATGACCTTGC CCACAGCCTT (R).

RPL18: GCAAGCCAGCACTGAATACG (F); TGCTGGCACTC AGGATGGTT (R).

Tubulin: TGTCGCGTGTGAAACACTTC (F); AGCAGGCGTTT CCAATCTG (R).

RPL32: ATGCTAAGCTGTCGCACAAATG (F); GTTCGATCCGT AACCGATGT (R).

Actin: ATGTGCAAGGCCGGTTTCGC (F); CGACACGCAGCT CATTGTAG (R).

2.3.3.2 | *dFmr1, Noncanonical FMRpolyG-GFP and Canonical GFP Protein Levels Measurement.* To evaluate the effect of PIP NPs on the dFmr1, noncanonical FMRpolyG-GFP, and canonical GFP protein levels in the CGG repeat *Drosophila*, *Drosophila* heads

collected previously were subjected to protein extraction (30 heads per test, total 90 heads for three independent biological replicates) using the SDS Lysis Buffer (Beyotime, China) containing BeyoZonase Super Nuclease (Beyotime, China), Protease inhibitor cocktail (Beyotime, China), and Phosphatase Inhibitor Cocktail (CWBIO, China) according to the instructions from manufacturers. The total protein was separated using a 4%–12% FuturePAGE gel (ACE Biotec, China) and then transferred to polyvinylidene fluoride (PVDF) membranes (Merck Millipore, Germany). The PVDF membranes were blocked with NcmBlot Blocking Buffer (NCM biotech, China). To monitor dFmr1 and FMRpolyG protein levels, the membranes were incubated with primary antibodies against FMRP (A4539, 1:500, ABclonal, China) or FMRpolyG (MABN1788, 9FM-1B7, 1:2000, Sigma–Aldrich, USA) overnight at 4 °C. Although the anti-FMRP antibody was raised against human FMRP, this antibody detected a specific band at approximately 83 kDa in *Drosophila* lysates, corresponding to the molecular weight of the endogenous dFmr1, and showed treatment-dependent expression changes. After being washed several times in PBST, the membranes were then incubated with HRP-conjugated goat anti-rabbit secondary antibody (AS014, 1:10,000, ABclonal, China) or HRP-conjugated goat anti-mouse secondary antibody (AS003, 1:10,000, ABclonal, China) at room temperature for 1 h. After monitoring the protein bands of dFmr1 and FMRpolyG protein, the antibodies on the PVDF membranes removed using a fast Western blot antibody stripping buffer (Vazyme, China), followed by incubation with primary antibodies against GFP (AE012, 1:5000, ABclonal, China) or beta-actin (AC026, 1:10,000, ABclonal, China) overnight at 4 °C and HRP-conjugated goat anti-rabbit secondary antibody (AS014, 1:10,000, ABclonal, China) or HRP-conjugated goat anti-mouse secondary antibody (AS003, 1:10,000, ABclonal, China), as an internal control to standardize the difference. The protein bands on the PVDF membranes were visualized using a ChemiDoc MP imaging system (Bio-Rad, Singapore) and quantified using ImageLab 6.1 software (Bio-Rad, USA).

2.3.3.3 | *Presence of Ubiquitin-Positive Intranuclear Inclusions.* We conducted an immunofluorescence analysis to evaluate the effect of PIP NPs on the presence of ubiquitin-positive intranuclear inclusions in the entire brain hemisphere (including optic lobe and central brain) of *elav* > CGG_{90} (3 fields of view (FOV) per brain from 3 heads for total of 9 FOV from three independent biological replicates) and eye of *GMR* > CGG_{90} *Drosophila* (3 fields of view (FOV) per eye from 3 heads for total of 9 FOV from three independent biological replicates). After fixation at 4 °C overnight, the *Drosophila* heads collected previously were rinsed several times in PBS, and then immersed in 30% sucrose-PBS solution at 4 °C for 24 h. The treated *Drosophila* heads were frozen in an optimal cutting temperature (OCT) compound (Sakura Finetek, Japan). The frozen OCT blocks were cryosectioned (12 μm thickness) using a Leica CM 1950 cryostat (Leica, US), placed on slides, and stored at −80 °C until analyses. The sections were treated with quick antigen retrieval solution for frozen sections (Beyotime, China) for 5 min and rinsed several times in PBS, followed by blocking and permeabilization in blocking buffer (5% bovine serum albumin and 0.3% Triton ×100 (Bidepharm, China) in 1× phosphate-buffered saline at room temperature for 60 min. After rinsing several times in PBS, the sections were incubated with an anti-mouse primary antibody against ubiquitin (sc-8017, 1:200, Santa Cruz Biotechnology, USA) overnight at 4 °C, rinse several times in PBS, followed by incubation with an goat anti-mouse secondary antibody with Alexa Fluor 647 (A32728TR, 1:200, Abcam, USA) for 1 h at room temperature in a light-proof humidified chamber. All slides were treated with an antifade mounting medium containing DAPI (Beyotime, China) and covered with coverslips. Fluorescence imaging was performed under a Nikon ECLIPSE Ti fluorescence microscope (Nikon, Japan). The number of nuclei and ubiquitin-positive intranuclear inclusions was calculated with FIJI ImageJ software (https://imagej.net/software/fiji/). For quantitative analyses, DAPI-stained nuclei were segmented and counted using the StarDist 2D plugin in Fiji [24] using the default pretrained model to ensure unbiased nuclear segmentation and inclusion counting. Nuclear boundaries were defined based on DAPI staining. Any ubiquitin fluorescence falling outside the DAPI-defined nuclear mask was considered background and excluded from quantification. The percentage of nuclei containing ubiquitin inclusions was calculated using the following equation, as previously described [4].

$$\text{Nucleiwithubiquitin inclusion}(\%) = \frac{\text{ubiquitin positive intranuclear inclusions}}{\text{DAPI positive nuclei}} \times 100\%$$

2.4 | Effect of PIP NPs on Behavior in CGG Repeat Mice

2.4.1 | *Preparation of CGG Repeat Mice*

2.4.1.1 | *Source of Mice.* B6.129P2(Cg)-*Fmr1*tm2Cgr/DlnJ mice were bought from the Jackson Laboratory. The mutant and their wildtype littermates (WT) aged 50–54 weeks old were supplied by the Laboratory Animal Services Center of The Chinese University of Hong Kong. Mice were housed in a temperature-controlled room (22 ± 2 °C) under a 12 h light/dark cycle with *ad libitum* access to food and water. Based on prior experience, minimally necessary mice were randomly allocated to experimental groups. Behavioral parameters were acquired and analyzed via Smart 3.0 software (PanLab, Barcelona, Spain), and histological quantifications were performed using automated nuclear segmentation (StarDist 2D plugin in Fiji) with random field-of-view selection, thereby eliminating observer bias at the data acquisition and analysis levels.

All animal-related experimental procedures strictly adhered to the guidelines outlined in the Guide for the Care and Use of Laboratory Animals issued by the U.S. National Institutes of Health [25]. The research protocol was reviewed and approved by the Animal Ethics Committee of The Chinese University of Hong Kong (Approval No.: 20-035-GRF).

2.4.1.2 | *Genotyping.* Genotyping was performed on mice at 2 weeks of age. Briefly, DNA was extracted from mouse tails using a quick genotyping assay kit for mouse tail (Beyotime, China) according to the instructions from the manufacturer. The forward primer was 5′-GTC AGC GAA GCG GGA ATG-3′, and the reverse primer was 5′-CAC TGG GAG AGG ATT ATT TG-3′. PCR was conducted using the Applied Biosystems MiniAmp Plus thermal cycler (Applied Biosystems, CA, USA) under the

following thermal cycling conditions: initial denaturation at 94 °C for 3 min (one cycle), followed by 30 cycles of denaturation at 94 °C for 30 s, annealing at 55 °C for 30 s, and extension at 72 °C for 20 s. Subsequently, a final extension (one cycle) was performed at 72 °C for 10 min. DNA band sizes were determined by running DNA samples on a 2.5% agarose gel containing SYBR-safe DNA gel stain (Invitrogen, CA, USA). DNA bands were visualized using a ChemiDoc MP imaging system (Bio-Rad, Singapore).

2.4.1.3 | *Verification of Motor Coordination.* To establish the CGG repeat mice model for evaluating motor coordination, male CGG repeat mice (mutant, $n = 7$) and WT mice ($n = 3$) aged 50–54 weeks were used. The motor coordination of mice was tested via a rotarod test (LE8205, PanLab, Harvard Apparatus, USA). Both training and test sessions were conducted 1 h after drug or vehicle administration. A total of two training sessions were conducted on one and 2 days before the test session. In the training session, each mouse was forced to walk on the rotating rod at a constant speed of 4 rpm. To ensure adequate familiarization, a training criterion was established, whereby mice had to remain on the rotating rod at a constant speed of 4 rpm for 60 consecutive seconds. Mice that met this criterion were subjected to the motor coordination test [26]. During the test session, the mice were placed on the rotating rod as the rotation speed gradually increased from 4 to 40 rpm over 300 s with an acceleration rate of 7.2 rpm/min [27]. Each mouse was tested five times, with a minimum interval of 10 min between trials to prevent fatigue [27]. The latency to fall was recorded, with the highest and lowest values excluded before data analysis. A significant difference in the latency of fall between WT and mutant mice was considered to demonstrate the successful development of the model for testing motor coordination.

2.4.1.4 | *Verification of Learning and Memory Ability.* The same cohort of mice used in the verification of motor coordination was subjected to learning and memory ability testing after a 3-day rest period. The learning and memory abilities of the mice were tested via a Barnes maze test, as previously described [28]. Testing consisted of two trials per day over four consecutive days. Briefly, a 92 cm diameter circular platform with twenty 5 cm holes along the perimeter was utilized. Each trial began with the mouse placed in a 7.5 cm cylindrical chamber at the maze center. After 10 s, the chamber was removed, and the mouse was allowed to explore the maze freely. The trial ended when the mouse entered the goal tunnel or after 5 min. The mouse was allowed to remain in the tunnel for 1 min. The time taken to reach the goal tunnel was recorded. A significant difference in the time taken to reach the goal tunnel between wild-type and mutant mice was considered to demonstrate the successful development of the model for testing learning and memory abilities.

2.4.2 | *Evaluation of PIP NPs Maximum Tolerated Dose (MTD) in CGG Repeat Mice*

Both female and male CGG repeat mice were used to determine the multiple dose MTD of PIP NPs. In the first cohort, female wild-type (WT) mice ($n = 3$) were orally administered PIP NPs at a dose of 40 mg/kg with a volume of 10 mL/kg body weight based on our previous experiments [16]. In the second cohort, female CGG repeat heterozygous mice were orally administered PIP NPs at a dose of 40 mg/kg ($n = 4$) or 30 mg/kg ($n = 4$) to refine the toxicity threshold in the disease background. In the third cohort, male CGG repeat mutant mice ($n = 3$) and wild-type mouse ($n = 1$) were given the PIP NPs treatments at three different doses of 20 mg/kg/day for the 1st week, 30 mg/kg/day for the 2nd week, and 40 mg/kg/day for the 3rd week by oral gavage once daily. The MTD was defined as the dose of PIP NPs that resulted in a body weight loss of more than 10% [29].

2.4.3 | *Treatment and Behavior Assessments*

The verified CGG repeat mice were randomly assigned into three groups (Groups I to III, $n = 10$/group), including Group I (negative control group): WT mice + vehicle, Group II (disease model control group): mutant CGG repeat mice + vehicle, and Group III (PIP NPs treatment group): mutant CGG repeat mice + PIP NPs. The mice were orally administered PIP NPs at the MTD or an equivalent volume of vehicle once daily for nine consecutive weeks.

As shown in Figure 2A, to evaluate the effect of PIP NPs on the locomotor performance and the motor coordination of CGG repeat mice, the accelerating rotarod was tested on the 2nd, 4th, 6th, and 8th weeks of treatment. The total distance in open field test (OFT), and the latency to fall between wild-type, vehicle-treated mutant and PIP NPs treated mutant mice were obtained and compared. Similarly, as shown in Figure 2A, to evaluate the effect of PIP NPs on the learning and memory abilities of CGG repeat mice, the Barnes maze was assessed on the 3rd, 5th, 7th, and 9th weeks of treatment. To minimize the influence of spatial memory cues, the platform rotated 90° clockwise before each testing session. The time taken to reach the goal tunnel between wild-type, vehicle-treated mutant and PIP NPs treated mutant mice was obtained and compared. Behavioral parameters were acquired and analyzed via Smart 3.0 software (PanLab, Barcelona, Spain) to minimize observer bias. At the end of the experiment, mice were deeply anesthetized with a mixture of ketamine (100 mg/kg) and xylazine (10 mg/kg) via intraperitoneal injection. Subsequently, they were intracardiac perfused with 25 mL of ice-cold PBS, followed by excising the whole brain. Subsequently, the brains were used for evaluating the mRNA and protein levels relative to FXTAS. For assessing the biomarker levels in the whole brain, the brains were divided into left and right hemispheres. The left hemisphere was immediately frozen in liquid nitrogen and stored at −80 °C for subsequent mRNA and protein extraction, while the right hemisphere was immersed in ice-cold 4% paraformaldehyde (Solarbio, China) for fixation. For evaluating the biomarker levels in different brain regions, the olfactory, basal ganglia, cortex, hypothalamus, thalamus, hippocampus, midbrain, cerebellum, pons, and medulla were dissected from the brains. The brain tissues designated for evaluating mRNA levels were immediately stored in ice-cold RNALater RNA Stabilization Reagent for Animal Tissue (Beyotime, China), while the tissues designated for extracting protein were immediately frozen in liquid nitrogen and stored at −80 °C.

2.4.4 | *Evaluation of FMR1 mRNA, FMRP, FMRpolyG Protein Level, and the Presence of Ubiquitin-Positive Intranuclear Inclusions*

2.4.4.1 | *FMR1 mRNA Level Measurement.* To evaluate the effect of PIP NPs on the *FMR1* mRNA levels in mouse models, mouse

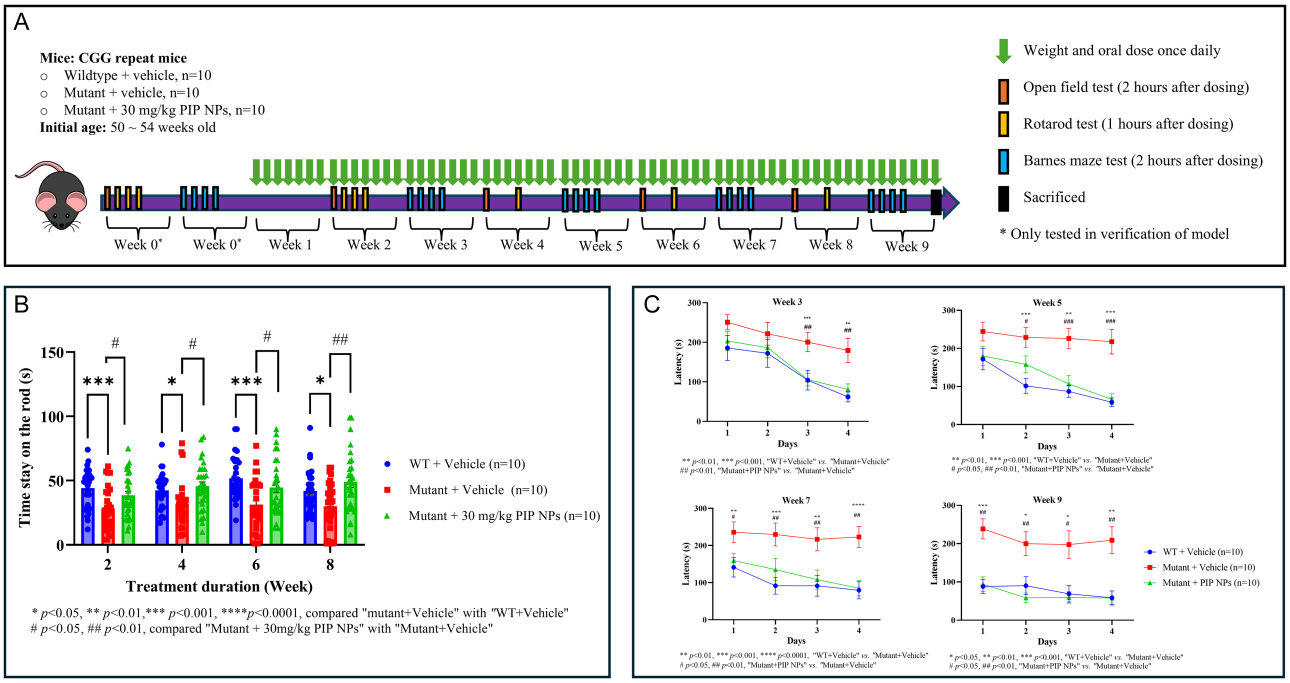

FIGURE 2 | Evaluation of behavioral improvements in CGG repeat mice following 9-week PIP NPs treatment. (A) Schematic diagram of the experimental grouping and timeline for the 9-week oral administration of PIP NPs (30 mg/kg). (B) Motor coordination assessment using the accelerating rotarod test ($n = 10$ per group). (C) Spatial learning and memory analysis using the Barnes maze test ($n = 10$ per group). Data was presented as mean ± SEM. Statistical significance was determined by two-way ANOVA (and two-way repeated-measures ANOVA for longitudinal behavioral datasets) followed by Tukey's post hoc test. *$p < 0.05$, **$p < 0.01$, ***$p < 0.001$, ****$p < 0.0001$; #$p < 0.05$, ##$p < 0.01$, and ###$p < 0.001$.

brains collected previously were subjected to total RNA extraction ($n = 6$ for whole brain and $n = 3$ for each of ten different brain regions) using an animal total RNA isolation kit (FOREGENE, Chengdu, China) according to the instructions from the manufacturer. The cDNA synthesis and qPCR amplification were conducted as previously described in Section 2.3.3.

Relative mRNA expression was normalized to an internal control to standardize the difference. The following primer sequences, reported previously [18, 30], were used in the study:

CGG repeat-specific primers: GCTCAGCTCCGTTTCGGTTT CACTTCCGGT (primer C); AGCCCCGCACTTCCACCACCAG CTCCTCCA (primer F).

GAPDH: GGAGCGAGATCCCTCCAAAAT (F); GGCTGTTGTC ATACTTCTCATGG (R).

2.4.4.2 | *FMRP and FMRpolyG Protein Level Measurement.* To evaluate the effect of PIP NPs on the FMRP and FMRpolyG protein level in the CGG repeat mice models, mouse brains collected previously were subjected to protein extraction and Western blot analyses, as detailed in Section 2.3.3. To monitor FMRP and FMRpolyG protein levels, the membranes were incubated with primary antibodies against FMRP (A4539, 1:1000, ABclonal, China) or FMRpolyG (MABN1788, 9FM-1B7, 1:2000, Sigma–Aldrich, USA) overnight at 4 °C. After being washed several times in PBST, the membranes were then incubated with an HRP-conjugated goat anti-rabbit secondary antibody (AS014, 1:10000, ABclonal, China) or an HRP-conjugated goat Anti-Mouse IgG (H&L) preadsorbed secondary antibody (ab97040, 1:10000, Abcam, USA) at room temperature for 1 h. After monitoring the protein bands of FMRpolyG protein, the antibodies on the PVDF membranes were removed using a fast Western blot antibody stripping buffer (Vazyme, China), followed by incubation with primary antibodies against beta-actin (AC026, 1:10,000, ABclonal, China) overnight at 4 °C and HRP-conjugated goat anti-rabbit secondary antibody (AS014, 1:10,000, ABclonal, China), as an internal control to standardize the difference. The protein bands on the PVDF membranes were visualized using a ChemiDoc MP imaging system (Bio-Rad, Singapore) and quantified using ImageLab 6.1 software (Bio-Rad, USA).

2.4.4.3 | *Presence of Ubiquitin-Positive Intranuclear Inclusions.* We conducted an immunofluorescence analysis to evaluate the effect of PIP NPs on the presence of ubiquitin-positive intranuclear inclusions in various brain regions of CGG repeat mice (3 FOV per region across ten different brain regions from 3 heads). Immunofluorescence staining was performed as previously described in Section 2.3.3. After blocking and permeabilization, the sections were incubated with an anti-ubiquitin primary antibody (ab7780, 1:200, Abcam, USA) overnight at 4 °C and rinsed several times in PBS, followed by incubation with a goat anti-rabbit secondary antibody conjugated to FITC (AS011, 1:200, ABclonal, China) for 1 h at room temperature in a light-proof humidified chamber. All slides were treated with an antifade mounting medium containing DAPI (Beyotime, China) and covered with coverslips. Fluorescence imaging was performed under a Nikon ECLIPSE Ti fluorescence microscope (Nikon, Japan). The number of nuclei and ubiquitin-positive intranuclear inclusions was calculated with FIJI ImageJ software (https://imagej.net/software/fiji/) using the StarDist 2D

plugin in Fiji [24], as described in Section 2.3.3 to ensure unbiased nuclear segmentation and inclusion counting. For quantification of nuclei with ubiquitin inclusions (%) across the whole mouse brain, the nuclei with ubiquitin inclusion (%) were quantified across ten different brain regions, aggregated to represent whole-brain values, and subsequently compared between experimental groups.

$$\text{Nucleiwithubiquitin inclusion}(\%) = \frac{\text{ubiquitin positive intranuclear inclusions}}{\text{DAPI positive nuclei}} \times 100\%$$

2.5 | Molecular Docking Analyses

Molecular docking was performed to explore how piperine interacted with specific proteins involved in *FMR1* transcript regulation (DHX9, a G-quadruplex and R-loop resolving helicase [31, 32]), the RAN translation of FMRpolyG (DAP5, an initiation factor of RAN translation [33]), and the clearance of ubiquitin-positive intranuclear inclusions (Hsp70, a heat shock protein that identified and cleared toxic proteins [34]) across three species of human, mouse, and *Drosophila*. The 3D structure of piperine was retrieved from PubChem (https://pubchem.ncbi.nlm.nih.gov/). The crystal structures of the target proteins were obtained from the RCSB Protein Data Bank (http://www.rcsb.org) or AlphaFold (https://alphafold.ebi.ac.uk/). Specifically, the human DHX9 (PDB ID: 8SZP) and the *Drosophila* ortholog MLE (PDB ID: 5AOR) were obtained from RCSB PDB, while the mouse DHX9 was obtained from the (AlphaFold ID: AF-O70133-3-F1-v6). The human DAP5 structure was retrieved from RCSB PDB (PDB ID: 4IUL). The mouse and *Drosophila* DAP5 structures were obtained from AlphaFold (AlphaFold ID: AF-Q62448-2-F1-v6) and (AlphaFold ID: AF-Q9VCH1-F1-v6), respectively. The latest human Hsp70 structure was obtained from RCSB PDB (PDB ID: 5AQZ, 1.65 Å) rather than the older Hsp70 structure (PDB ID: 1S3X, 2.60 Å) used in previous reports [35], while mouse and *Drosophila* Hsp70 structures were obtained from AlphaFold (AF-Q61696-F1-model_v6) and AF-P02825-F1-model_v6), respectively.

Prior to docking, all protein structures were optimized by removing water molecules, native ligands, and low-confidence disordered regions (for AlphaFold models) using PyMOL (version 3.1.6.1, DeLano Scientific LLC, USA) and by adding polar hydrogens and Gasteiger charges using MGLtools with AutoDock Tools (version 1.5.7, The Scripps Research Institute, USA). Molecular docking was performed to obtain the related docking affinities using AutoDock Vina (version 1.1.2, Scripps Research Institute, USA) as described previously [36]. The search grids for target proteins were defined as follows: the grids for DHX9 and MLE were centered on the native ADP-binding pocket within the helicase core to evaluate potential competitive binding; the grids for DAP5 and its orthologs were set to encompass the entire protein surface for a blind docking strategy; and the grids for Hsp70 were centered on the nucleotide-binding domain (NBD). The docking parameters were set with an exhaustiveness of 32. Interactions and binding types between piperine and proteins were visualized using PyMOL and Discovery Studio (version 25.1.0.24284, Dassault Systèmes, France).

2.6 | Data Analysis

Data was presented as mean±SEM. The concentration of piperine in the nanoparticles was determined in triplicate. For *Drosophila* and mouse studies, data represent results derived from at least three independent biological replicates or separate animal cohorts. All statistical analyses were performed using GraphPad Prism (version 9.5.1, GraphPad Software, La Jolla, CA). Data was analyzed using a one-way or two-way ANOVA (and two-way repeated-measures ANOVA for longitudinal behavioral datasets) followed by Tukey's post hoc test. A p-value of less than 0.05 was considered as statistically significant.

3 | Results

3.1 | Amelioration of Motor Dysfunction, Lifespan, and Retinal Degeneration by PIP NPs Treatment in CGG Repeat *Drosophila* via Reducing *FMR1* mRNA Levels, Restoring dFmr1 Levels, Decreasing Noncanonical FMRpolyG-GFP and Canonical GFP Protein Levels, and Reducing the Formation of UbiquitIn-Positive Intranuclear Inclusions

3.1.1 | PIP NPs Improved Locomotor Deficits, Retinal Degeneration, and Lifespan in CGG_{90} Drosophila

Before evaluating the therapeutic efficacy in vivo, we verified the characterization of the PIP NPs with uniform particle size of 205.02±4.66 nm (PDI: 0.24±0.03) and a zeta potential of −22.49 mV, which were consistent with our previous findings [16].

As shown in Figure 1B, flies expressing 90 CGG repeats (*elav* > CGG_{90}) exhibited a significantly higher climbing failure rate compared to that from wild-type controls ($p < 0.0001$), confirming the validity of the *elav* > CGG_{90} model. It is noted that treatment with PIP NPs significantly ameliorated the locomotor deficit ($p < 0.05$ to $p < 0.0001$) compared to that from the vehicle-treated group (Figure 1B), demonstrating a significant restoration of motor function upon PIP NPs treatment. As shown in Figure 1C, observations of lifespan under optimized conditions of 29 °C growing environment with twice-weekly food changes demonstrated that the *elav* > CGG_{90} flies showed significantly shortened survival compared to controls ($p < 0.0001$), suggesting the model establishment of *elav* > CGG_{90} flies. Notably, treatment with 100 μM PIP NPs significantly protected against early-stage mortality, particularly during the first 10 days ($p < 0.05$). Despite this significant impact on *elav* > CGG_{90} flies, treatment with 100 μM PIP NPs did not significantly affect climbing ability (Figure S1A) and survival rates (Figure S1B) in WT flies.

Furthermore, we assessed retinal integrity using the pseudopupil assay. Typically, a healthy ommatidium displays seven visible rhabdomeres. In contrast, the *GMR* > CGG_{90} model of retinal degeneration exhibited a loss of these structures, characterized by a significantly reduced number of rhabdomeres per ommatidium compared to controls ($p < 0.0001$). Notably, PIP NP treatment at all tested doses (5, 50, and 100 μM) significantly preserved retinal structure and increased rhabdomere counts ($p < 0.0001$), as shown in Figure 1D, indicating the protected effect against retinal degeneration by PIP NPs in CGG repeat flies.

3.1.2 | *PIP NPs Reduced Toxic Markers in CGG_{90} Drosophila*

In both fly models, *FMR1* mRNA level was significantly increased (Figure 3A, $p < 0.01$ and $p < 0.0001$, respectively), with increased canonical GFP (Figure 3C, $p < 0.0001$) and noncanonical FMRpolyG-GFP proteins (Figure 3D, $p < 0.001$ to $p < 0.0001$) compared with those from the control flies. PIP NPs treatment significantly lowered the high *FMR1* mRNA levels (Figure 3A, $p < 0.05$ for PIP NPs in $elav > CGG_{90}$; $p < 0.01$ to $p < 0.001$ for PIP NPs treatments in $GMR > CGG_{90}$). Using an antibody against mammalian FMRP, which cross-reacts with the *Drosophila* ortholog, we identified endogenous dFmr1 as a ~83 kDa band. The dFmr1 protein was significantly decreased in the CGG repeat fly models (Figure 3B, $p < 0.05$ for $elav > CGG_{90}$ and $p < 0.01$ for $GMR > CGG_{90}$) and was restored by PIP NPs treatment (Figure 3B, $p < 0.05$ to $p < 0.01$ for PIP NPs treatments in $elav > CGG_{90}$; $p < 0.01$ for PIP NPs treatments in $GMR > CGG_{90}$). PIP NPs treatment significantly reduced the reporter canonical GFP reporter signal (Figure 3C, $p < 0.05$ for PIP NPs treatments in $elav > CGG_{90}$; $p < 0.05$ to $p < 0.01$ for PIP NPs treatments in $GMR > CGG_{90}$). Similarly, the level of RAN-translated FMRpolyG-GFP was significantly decreased (Figure 3D, $p < 0.05$ to $p < 0.01$ for PIP NPs treatments in $elav > CGG_{90}$; $p < 0.05$ to $p < 0.01$ for PIP NPs treatments in $GMR > CGG_{90}$). Notably, while PIP NPs treatment significantly reduced the levels of toxic markers compared to the vehicle group, no statistically significant differences were observed among the three dosage groups. Finally, we examined the presence of ubiquitin-positive intranuclear inclusions. While untreated diseased flies had widespread ubiquitin-positive inclusions compared to WT flies, PIP NP treatment significantly reduced the percentage of nuclei containing these inclusions at all doses (Figures 3E, S2, and S3, $p < 0.0001$). No statistically significant differences were observed among the three dosage groups.

3.2 | Amelioration of Motor Coordination and Learning Ability by PIP NPs Treatment via Reducing *FMR1* mRNA Levels, Restoring FMRP Levels, and Reducing the Formation of Ubiquitin-Positive Intranuclear Inclusions in CGG Repeat Mice

3.2.1 | *Safety and Behavioral Improvements in Mice*

First, we determined the safe dose of PIP NPs in CGG repeat mice. The dose of 30 mg/kg was selected as the MTD, as it maintained good tolerability over the treatment period. No significant adverse effects were observed after treatment with PIP NPs at doses of 20 and 30 mg/kg in the CGG repeat mice. In contrast, oral administration of 40 mg/kg for five consecutive days led to a body weight loss exceeding 10%, indicating dose-limiting toxicity at this level. In addition, mice treated with 40 mg/kg exhibited reduced spontaneous locomotor activity lasting approximately 1 h postdosing, further suggesting the behavioral suppression at this dose. Therefore, we selected 30 mg/kg as the MTD dose for PIP NPs treatment. Following 9 weeks of treatment with PIP NPs at 30 mg/kg, body weight of the treated mice changes remained within 10% of baseline (day 0). No abnormal behavior was observed for 30 min postdosing, and no treatment-limiting adverse effects were detected throughout the study.

We then tested motor coordination using the rotarod test. As shown in Figure 2B, during the 9 week testing period, the vehicle-treated CGG repeat mice displayed impaired motor coordination compared to WT mice ($p < 0.05$ to $p < 0.001$), confirming the validity of the model. Compared with vehicle-treated CGG KI mice, PIP NP-treated mice showed significantly improved motor coordination across testing weeks, as evidenced by increased latency to fall (Figure 2B, $p < 0.05$ for week 2–6, and $p < 0.01$ for week 8). Importantly, to ensure that cognitive evaluations were not confounded by reduced locomotor performance, an OFT was conducted. The OFT data (Figure S4) showed no significant differences in total locomotor distance between WT and mutant mice, confirming that base locomotor performance was unaffected and that subsequent Barnes maze escape latencies reflected genuine cognitive and spatial memory deficits in CGG repeat mice. The learning ability of the CGG repeat mice was further tested using the Barnes maze. The CGG repeat mice took longer to find the escape tunnel compared with the WT mice on day 4 (Figure 2C, $p < 0.01$ to $p < 0.0001$), indicating these spatial learning deficits. Treatment with PIP NPs significantly shortened the latency for the mice to find the escape tunnel on day 4 from week 3 to week 9 (Figure 2C, $p < 0.01$ to $p < 0.0001$), indicating better memory and learning.

3.2.2 | *PIP NPs Restored FMRP and Reduced the Presence of Ubiquitin-Positive Intranuclear in Mice*

In the whole brain, CGG KI mice exhibited elevated *FMR1* mRNA levels (Figure 4A, $p < 0.01$) and reduced FMRP levels compared with WT (Figure 4B, $p < 0.01$). PIP NP treatment significantly decreased *FMR1* mRNA (Figure 4A, $p < 0.05$) and restored FMRP expression (Figure 4B, $p < 0.05$). To further assess regional consistency, *FMR1* mRNA and FMRP levels were quantified across ten distinct brain regions: olfactory, basal ganglia, cortex, hypothalamus, thalamus, hippocampus, midbrain, cerebellum, pons, and medulla. Region-wise analyses showed significantly increased *FMR1* mRNA levels (Figure 4A, $p < 0.01$ to $p < 0.0001$) and reduced FMRP levels in CGG repeat mice compared with WT mice across all regions (Figure 4B, $p < 0.01$ to $p < 0.001$), consistent with whole-brain findings. PIP NP treatment significantly decreased *FMR1* mRNA levels (Figure 4A, $p < 0.05$ to $p < 0.001$) and restored FMRP levels (Figure 4B, $p < 0.05$ to $p < 0.001$) across each region, with no significant interregional differences observed within groups, indicating a widespread and uniform therapeutic effect.

Moreover, the presence of ubiquitin-positive intranuclear inclusions was significantly elevated in the whole-brain of CGG repeat mice compared with WT mice (Figure 4C, $p < 0.0001$). PIP NP treatment markedly reduced the percentage of nuclei with ubiquitin-positive intranuclear inclusions (Figure 4C, $p < 0.0001$). Consistent with whole-brain findings, region-wise analyses revealed that CGG repeat mice exhibited significantly elevated levels of ubiquitin-positive intranuclear inclusions across all examined brain regions compared with wild-type controls (Figures 4C, S5, and S14, $p < 0.0001$). PIP NP treatment significantly reduced the percentage of nuclei with ubiquitin inclusions in all examined brain regions (Figures 4C, S5, and S14, $p < 0.05$ for hippocampus (Figure S10), midbrain (Figure S11), cerebellum (Figure S12), and medulla (Figure S14),

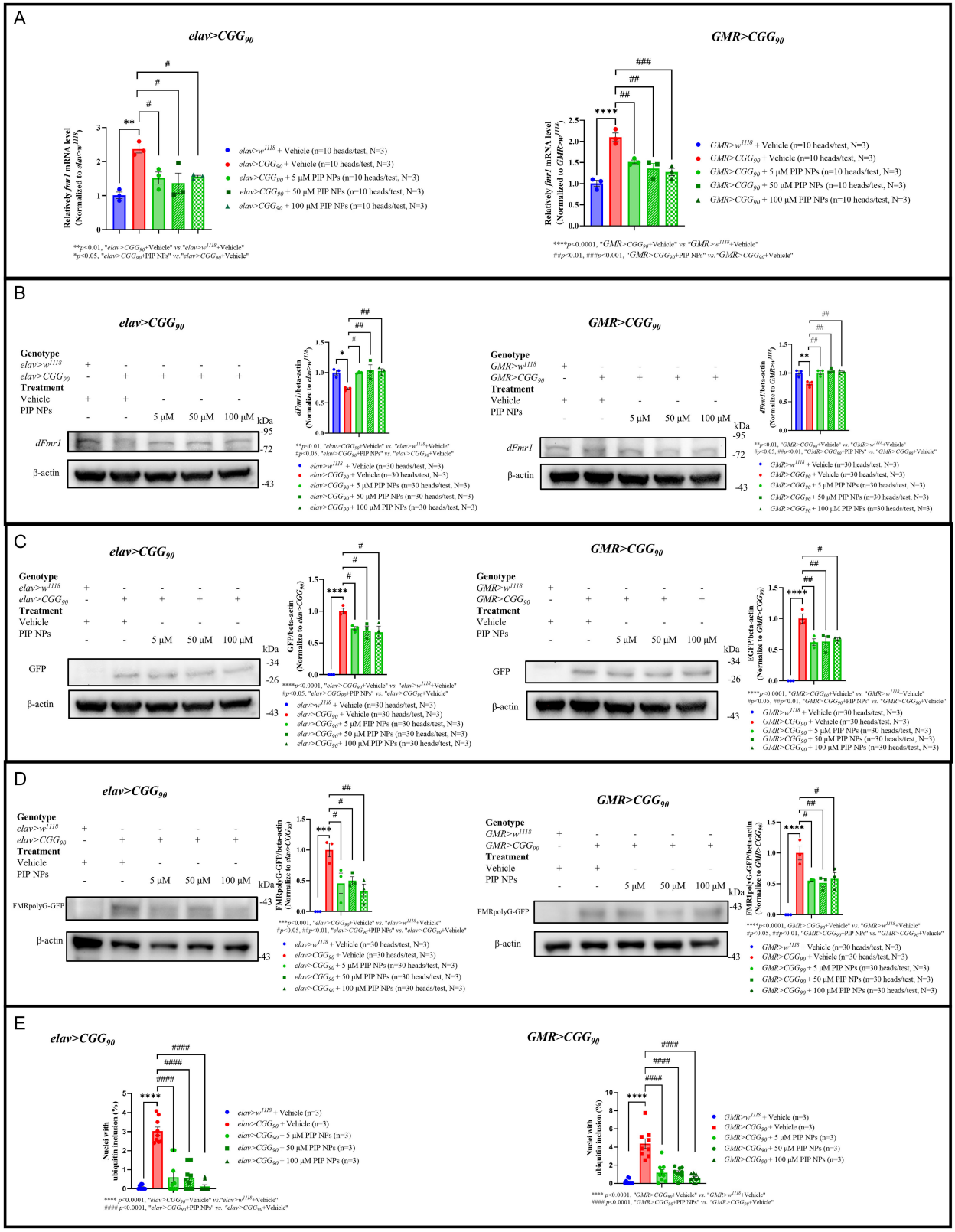

FIGURE 3 | Effects of PIP NPs at 5, 50, and 100 μM on the (A) *FMR1* mRNA level (10 heads per sample for three independent biological replicates); (B) dFmr1 level (30 heads per sample for three independent biological replicates); (C) canonical GFP protein level (30 heads per sample for three independent biological replicates); (D) noncanonical FMRpolyG-GFP protein level (30 heads per sample for three independent biological replicates); and (E) presence of ubiquitin-positive intranuclear inclusions in the head of *elav > CGG*$_{90}$ (Left) and *GMR > CGG*$_{90}$ (Right) *Drosophila*. Data was presented as mean ± SEM. Statistical significance was determined by one-way ANOVA followed by Tukey's post hoc test. *$p < 0.05$, **$p < 0.01$, ***$p < 0.001$, ****$p < 0.0001$; #$p < 0.05$, ##$p < 0.01$, ###$p < 0.001$, and ####$p < 0.0001$.

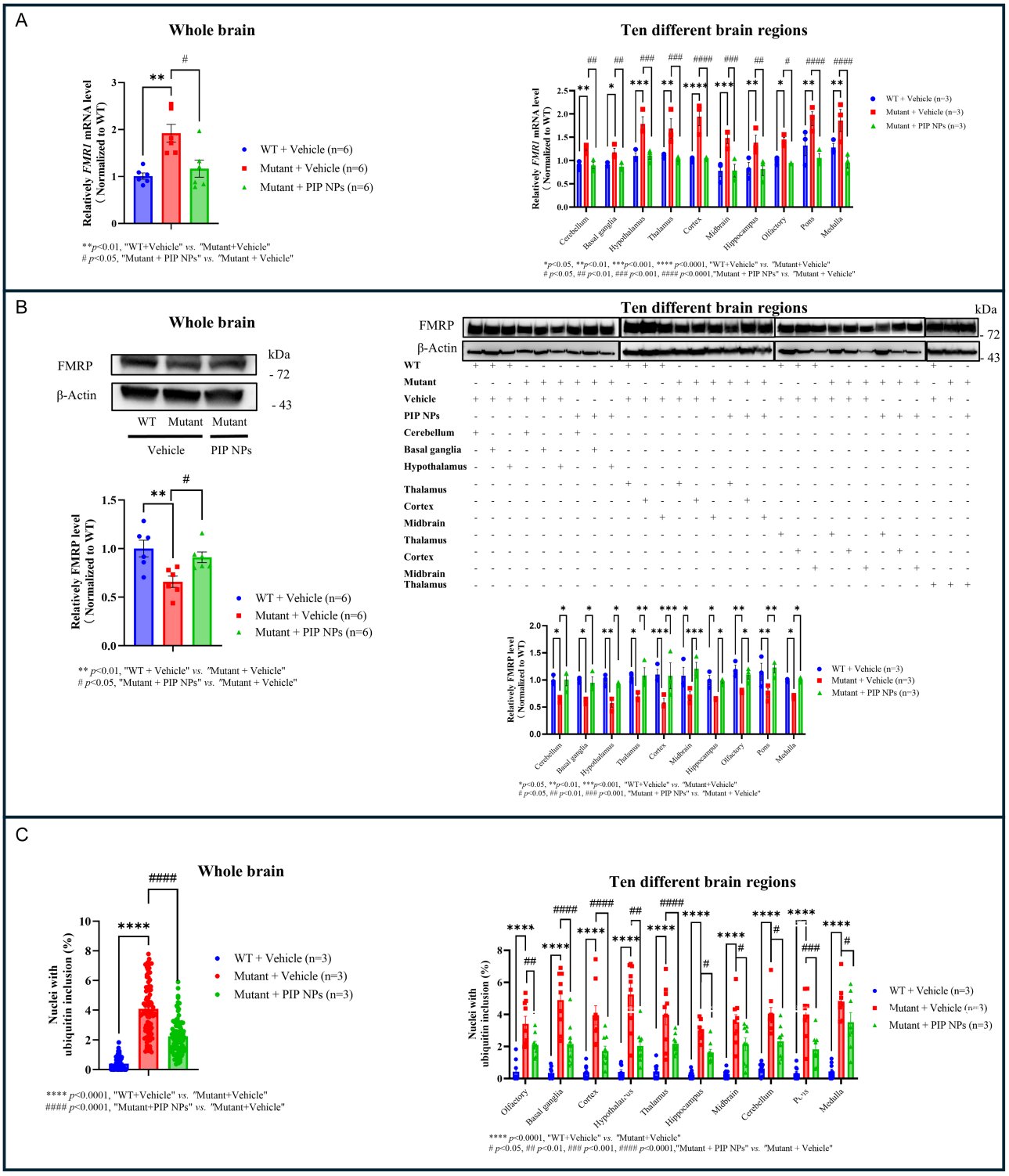

FIGURE 4 | Effects of 9 week oral treatment with PIP NPs at 30 mg/kg on the (A) *FMR1* mRNA level ($n = 6$ biologically independent animals for whole brain of mice, $n = 3$ biologically independent animals for each of ten different brain regions); (B) FMRP protein level ($n = 6$ biologically independent animals for whole brain of mice, $n = 3$ biologically independent animals for each of ten different brain regions); and (C) presence of ubiquitin-positive intranuclear inclusions in the whole brain (left) and ten different brain regions (right) of CGG repeat mice. Data was presented as mean±SEM. Statistical significance was determined by one-way ANOVA followed by Tukey's post hoc test. *$p < 0.05$, **$p < 0.01$, ***$p < 0.001$, ****$p < 0.0001$; #$p < 0.05$, ##$p < 0.01$, ###$p < 0.001$, and ####$p < 0.0001$.

$p < 0.01$ for olfactory (Figure S5) and hypothalamus (Figure S8), $p < 0.001$ for pons (Figure S13), and $p < 0.0001$ for basal ganglia (Figure S6), cortex (Figure S7), and thalamus (Figure S9), with no significant interregional differences observed within groups. These results indicated that the pathological accumulation of ubiquitin inclusions in CGG repeat mice was widespread throughout the brain and broadly responsive to PIP NP intervention.

3.3 | Multitarget Interactions of Piperine via Molecular Docking

Table 1 showed that piperine targeted identical binding domains with different affinities and interacting residues through a combination of hydrogen (H-bond), hydrophobic (Alkyl, π-Akyl, and π-Stack), and electrostatic (Cation, π-Cation, and π-Anion) bindings across all three species. Specifically, regarding DHX9 or its ortholog MLE, docking simulations against the helicase core domain of DHX9 revealed consistent binding of piperine with affinities of −7.6, −6.8, and −7.9 kcal/mol, across human (via hydrogen bonds and hydrophobic interactions), mouse (via hydrogen bonds and hydrophobic interactions), and *Drosophila* (via hydrogen bonds, hydrophobic interactions, and electrostatic interactions), respectively. Regarding the DAP5 or its ortholog, piperine docked effectively into the MIF4G domain of DAP5 across human (via hydrogen bonds, hydrophobic interactions, and electrostatic interactions), mouse (via hydrophobic interactions), and *Drosophila* (via hydrogen bonds and hydrophobic interactions), with binding affinities of −7.2, −6.7, and −7.9 kcal/mol, respectively. As to the Hsp70, piperine demonstrated high binding affinity toward the NBD of Hsp70 across human (via hydrogen bonds and electrostatic interactions), mouse (via hydrogen bonds and electrostatic interactions), and *Drosophila* (via hydrophobic interactions and electrostatic interactions), with binding affinities of −8.7, −9.0, and −8.1 kcal/mol, respectively.

In addition, Figure 5 illustrated the 3D docking poses of piperine with these three FXTAS-associated targets. Specifically, piperine occupied the deep hydrophobic pocket of the helicase core in DHX9 (human/mouse) and its ortholog MLE (*Drosophila*), bound to the MIF4G domain of DAP5 (human/mouse) and eIF4G2 (*Drosophila*), which is required for the recruitment of translation initiation factors (eIF4A). It is also noted that piperine could anchor to the conserved phosphate-binding loop within the NBD of Hsp70, which mimicked the ADP-bound state as described before [35].

In summary, these docking results provided a computational structural rationale for the proposed multitarget activity of piperine. The simulations suggested that piperine might simultaneously target genomic stability (DHX9) of *FMR1* gene, toxic translation of FMRpolyG (DAP5), and clearance of ubiquitin-positive intranuclear inclusions (Hsp70).

4 | Discussion

FXTAS is a progressive neurodegenerative disorder characterized by tremors, balance problems, and memory loss. Despite the severity of these symptoms, clinical management is currently limited to symptomatic treatment, with no disease-modifying therapies available to halt neurodegeneration. To address this critical therapeutic gap, our current study provided the first in vivo evidence that PIP NPs alleviated behavioral and pathological hallmarks in both CGG repeat *Drosophila* and mouse models. Specifically, the *elav > CGG$_{90}$ Drosophila* exhibited locomotor impairments, and *GMR > CGG$_{90}$ Drosophila* exhibited retinal degeneration [18]. For the model establishment of retinal degeneration, monitoring external eye morphology posed challenges

TABLE 1 | Piperine targeted identical binding domain with different affinities, interacting residues, and binding types across all three species.

Target protein	Species	Affinity, kcal/mol	Binding domain (residue range)	Interacting residues (types of binding)
DHX9/ MLE	Human	−7.6	Helicase core (398–809)	Trp660 (π-stack); Asn661 (H-bond); Tyr664 (π-stack)
	Mouse	−6.8	Helicase core (400–811)	Trp446 (π-alkyl); Thr451 (H-bond); Phe679 (C—H bond); Ile680 (alkyl); Ser681 (H-bond); Lys684 (π-alkyl)
	Drosophila	−7.9	Helicase core (394–813)	Leu384 (alkyl); Ser448 (H-bond); Glu451 (C—H bond); Arg455 (π-cation); Phe703 (π-Stack)
DAP5/ eIF4G2	Human	−7.2	MIF4G (78–308)	Lys233 (π-alkyl/cation); Leu236 (alkyl); Leu273 (alkyl/π-alkyl); Gln276 (H-bond); Tyr277 (π-alkyl); Arg280 (alkyl)
	Mouse	−6.7	MIF4G (78–308)	His229 (π-stack); Lys233 (alkyl/π-Alkyl); Leu236 (alkyl); Leu273 (alkyl); Tyr277 (π-alkyl); Arg280 (alkyl)
	Drosophila	−7.9	MIF4G (1340–1480)	Asn1364 (H-bond); Ile1414 (π-alkyl); Arg1427 (H-bond/π-alkyl); Cys1431 (π-sulfur)
Hsp70	Human	−8.7	NBD (2–386)	Thr13 (H-bond); Thr14 (H-bond); Tyr15 (H-bond); Asp366 (π-anion)
	Mouse	−9.0	NBD (2–386)	Thr13 (H-bond); Thr14 (H-bond); Thr15 (H-bond); Arg272 (π-cation); Arg342 (π-cation); Asp366 (π-anion)
	Drosophila	−8.1	NBD (2–386)	Tyr12 (π-stack); Arg270 (π-cation); Val367 (alkyl)

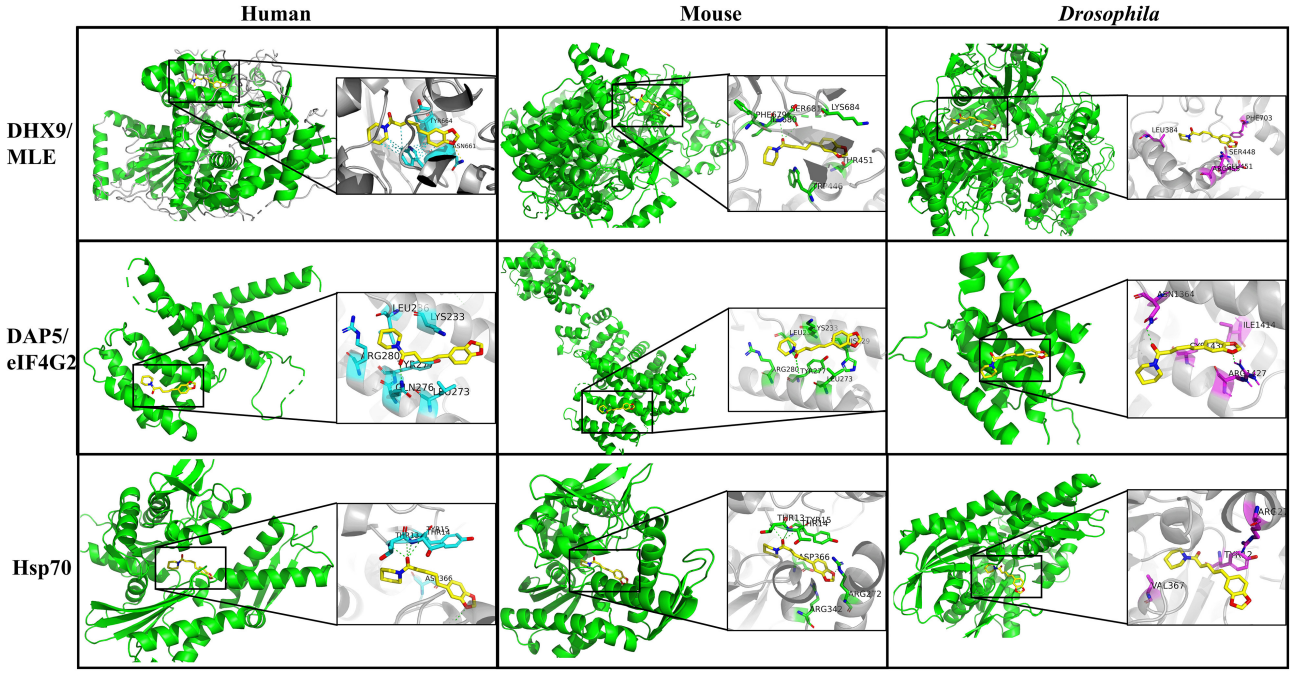

FIGURE 5 | Molecular docking analysis of piperine with FXTAS-associated targets via 3D docking pose across human, mouse, and *Drosophila*: DHX9 (human/mouse) and its ortholog MLE (*Drosophila*); DAP5 (human/mouse) and its ortholog eIF4G2 (*Drosophila*); and Hsp70. The columns correspond to the species (human, mouse, and *Drosophila*).

due to the subtle nature of retinal degeneration and the difficulty in quantitative assessment. To overcome this limitation, we adapted the pseudopupil assay to evaluate the extent of retinal degeneration in *GMR > CGG*$_{90}$ *Drosophila*. After the treatment, PIP NPs significantly improved locomotion, survival, and retinal integrity in the *Drosophila* model, while enhancing motor coordination and spatial learning in mice model. Notably, the locomotor performance of the mutant mice remained intact as confirmed by our OFT, suggesting that the observed therapeutic improvements in the Barnes maze specifically reflect the amelioration of spatial memory and cognitive deficits, independent of physical mobility. At the molecular level, PIP NPs can modulate the molecular hallmarks by lowering *FMR1* mRNA, restoring dFmr1 or FMRP expression across species, and decreasing the expression of FMRpolyG-GFP in *Drosophila*.

Extending beyond the *FMR1* mRNA and FMRpolyG protein, we further confirmed that the reduction in toxic RNA and protein successfully translated into the clearance of ubiquitin-positive inclusions. These ubiquitin-positive inclusions represent complex aggregates comprising FMRpolyG, expanded *FMR1* mRNA, and various sequestered RNA-binding proteins [37], serving as a translationally relevant pathological endpoint for FXTAS [21, 38]. It is worth noting that the age-dependent accumulation of ubiquitinated protein aggregates in the cytoplasm have been observed in the wild-type of both *Drosophila* [39–41] and mice [42, 43]. In addition, due to the increased monoubiquitinated histone H2A (ubH2A) with age, the ubiquitin signal within the nuclei of WT controls in both wild-type *Drosophila* and mice has been reported in previous studies [44, 45]. Nevertheless, significantly denser ubiquitin signals were observed in the CGG models than those in WT groups, demonstrating the ubiquitin antibody specificity. To filter out the ubiquitin signals in cytoplasmic background, overcome the limitations of traditional manual counting, and ensure the accurate counting of ubiquitin-positive intranuclear inclusions, we adopted the StarDist 2D plugin in Fiji for automated and unbiased nuclear segmentation and inclusion counting. Furthermore, we chose to use ubiquitin single-labeling without FMRpolyG colabeling due to the background interference of GFP in the *Drosophila* model and endogenous mouse IgG in the mice model [46]. Beyond confirming the clearance of aggregates, we observed a regionally uniform expression of ubiquitin-positive intranuclear inclusions in CGG repeat mice, followed by a uniform reduction after PIP NP treatment. Although previous studies documented that ubiquitin-positive intranuclear inclusions were distributed across brain regions (including the olfactory, basal ganglia, cortex, hypothalamus, thalamus, hippocampus, midbrain, cerebellum, pons, and medulla) in CGG repeat mice, with percentage of nuclei containing ubiquitin inclusion ranging from 5% to 15% [21, 47], the systematic comparisons of ubiquitin-positive intranuclear inclusion expression across ten comprehensive brain regions (including the olfactory, basal ganglia, cortex, hypothalamus, thalamus, hippocampus, midbrain, cerebellum, pons, and medulla) were lacking. Our systematic quantification across ten brain regions provided a more holistic evaluation of the percentage of ubiquitin-positive intranuclear inclusions. Furthermore, our findings revealed a uniform therapeutic response following PIP NPs treatment. The observed uniform decreases in *FMR1* mRNA and ubiquitin inclusions, alongside the restoration of FMRP across all ten regions, directly correlate with our previous pharmacokinetic findings. We have demonstrated that orally administered piperine exhibited robust CNS penetration and maintained a highly uniform distribution profile across diverse brain structures [48], which collectively suggested that uniform distribution of piperine made it suitable for providing whole brain therapeutic coverage to efficiently clear widespread toxic aggregates in FXTAS. Collectively, our data for the first time demonstrated the coherence between

piperine brain distribution and its effect on the ubiquitin-positive intranuclear inclusions after oral PIP NPs treatment, which supported the further development of piperine as a potential therapeutic agent for FXTAS.

The therapeutic effects of PIP NPs observed in this study can be interpreted through several interconnected molecular mechanisms, as summarized in Figure 6. According to previous findings on FXTAS [3], elevated *FMR1* mRNA levels were a key molecular feature of its premutation state. Such upregulation of *FMR1* mRNA levels was often accompanied by normal to moderately reduced levels of FMRP, likely due to the sequestration of RNA-binding proteins and general translational inefficiency caused by the toxicity of expanded r(CGG) repeats. In parallel, expanded CGG repeats undergo RAN translation, producing toxic proteins such as FMRpolyG, as shown in Figure 6, leading to the formation of ubiquitin-positive intranuclear inclusions in the brain, a pathological hallmark of FXTAS-associated neurodegeneration. The distribution of these inclusions has been reported across multiple brain regions in CGG knock-in mice with varying repeat lengths [21, 47]. Although the current therapeutic strategies for FXTAS focused on blocking the translation of FMRpolyG to reduce RAN-translated protein toxicity, effective elimination of r(CGG)exp RNA toxicity had been considered lately [49].

While previous studies showed that piperine selectively bound to r(CGG)exp hairpins [12] and G4 structures [28] to directly impede translation via steric hindrance, our findings suggested a more comprehensive dual-action mechanism. First, our RT–qPCR data demonstrated a significant decrease in total *FMR1* mRNA levels, indicating that the reduction of toxic FMRpolyG was partially driven by the cleared upstream RNA template (a process strongly supported by the restoration of endogenous dFmr1 and FMRP expression). Second, building upon the r(CGG)exp hairpin binding properties of piperine [12], piperine may structurally lock the remaining r(CGG)exp repeats to obstruct RAN translation initiation, a mechanism indirectly supported by our observed decrease in FMRpolyG-GFP and ubiquitin-positive inclusions. The reduction of *FMR1* mRNA level was consistent with the previous observation, where 50 μM piperine treatment significantly reduced the expression of the downstream canonical product GFP [12]. The parallel reduction of both the RAN-translated FMRpolyG-GFP and the canonically translated GFP from the same transcript [50] suggested that piperine could reduce the expanded *FMR1* transcript so as to mitigate FXTAS-associated toxicity via reducing both RNA-foci formation and RAN-mediated protein accumulation. Such reduction in both *FMR1* mRNA and FMRpolyG-GFP toxicities by PIP NPs might explain the observed decrease in ubiquitin-positive intranuclear inclusions in CGG repeat *Drosophila* and mouse models, a pathological hallmark in both FXTAS patients and CGG repeat animal models [21]. As also shown in Figure 6, in addition to reducing the *FMR1* mRNA and FMRpolyG, PIP NP treatment was found to be able to restore the FMRP/dFmr1 levels via neutralization of RNA toxicity. Collectively, our findings indicated that PIP NPs could improve FXTAS pathology by directly mitigating the two core toxicities caused by expanded CGG repeats, namely, r(CGG)exp RNA toxicity and RAN-translated protein toxicity [38].

Furthermore, molecular docking simulations with DHX9, DAP5, and Hsp70 provided a structural rationale that aligned with our experimental findings. DHX9 activity was required to unwind G4 structures that otherwise block translation [31], while it had been reported to promote toxic R-loop accumulation under the

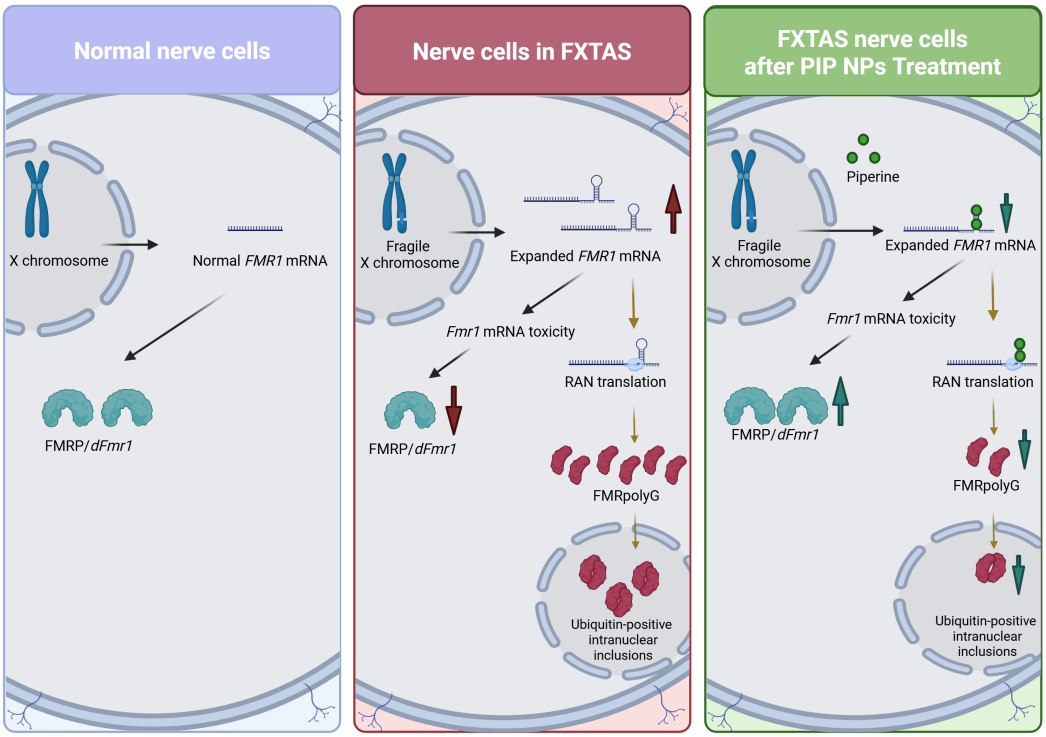

FIGURE 6 | Schematic illustration of the proposed therapeutic mechanisms of PIP NPs in FXTAS via decreasing *FMR1* mRNA, suppressing RAN translation, and decreasing ubiquitin-positive intranuclear inclusions.

condition of splicing dysfunction, a characteristic of FXTAS [32]. Our docking results suggested a potential inhibition of piperine toward DHX9/MLE via binding into its ATP-binding cleft, which may further hinder the DHX9-mediated aberrant R-loop formation [32] and prevent G4 unwinding [31]. These effects of piperine on DHX9, together with the direct stabilization of G4 structures by piperine [51], may lead to the downregulation and clearance of the toxic mRNA, resulting in the decreased *FMR1* mRNA levels, as observed in Figures 2A and 4A. Similarly, our docking analyses on DAP5 and Hsp70 suggested that piperine might sterically hinder the assembly of the FMRpolyG translation initiation complex and stabilize the chaperone in conformations within the NBD of Hsp70 that may facilitate the removal of ubiquitin-positive intranuclear inclusions, respectively. The MIF4G domain of DAP5 was essential for its interaction with key translation initiation factors [52]. Therefore, piperine binding at this site could disrupt these interactions, a mechanism consistent with recent findings that targeting DAP5 disrupted alternate translation modes [53], leading to the inhibition of FMRpolyG translation. It has also been noted that small molecules targeting the Hsp70 NBD could stabilize the molecular chaperone, leading to a high-affinity conformation of Hsp70 (ADP-bound state) [54]. Such conformation could promote the recognition and subsequent degradation of toxic substrates such as polyglutamine [55]. Therefore, it is considered that piperine might enhance the clearance of ubiquitin-positive intranuclear inclusions through its binding with Hsp70.

Several limitations of the present study should be noted. First, our current in silico molecular docking simulations aimed to provide a computational structural rationale for the potential interactions of piperine toward DHX9, DAP5, and Hsp70. However, the predicted binding affinities (Kd) and interactions of piperine toward DHX9, DAP5, and Hsp70 may require further verifications via surface plasmon resonance (SPR) spectroscopy and cellular thermal shift assay (CETSA) assays, respectively. Second, although our current studies demonstrated the MTD of PIP NPs and the stable body weight maintenance observed during the 9-week long-term efficacy treatment in the CGG repeat mice, a more comprehensive toxicology screening, including blood chemistry and tissue histopathology, remains an important direction for our long-term translational pipeline of PIP NPs.

5 | Conclusion

Our study demonstrated that treatment with PIP NPs protected against early-stage mortality of CGG repeat *Drosophila* and alleviated the locomotor deficits and retinal degeneration in these *Drosophila* models. Moreover, the treatment with PIP NPs also improved the motor coordination, learning, and memory abilities in the CGG repeat mice model. Mechanistically, our findings suggested that piperine acted as a multitarget modulator by reducing *FMR1* mRNA level, restoring dFmr1 or FMRP expression, and decreasing the FMRpolyG-GFP protein level (in *Drosophila*) and ubiquitin-positive intranuclear inclusions. Molecular docking simulations provided a computational structural rationale suggesting that piperine interacted with (1) DHX9 helicase to reduce *FMR1* transcript abundance; (2) DAP5 to suppress the RAN translation of FMRpolyG; and (3) Hsp70 to enhance the clearance of ubiquitin-positive intranuclear inclusions. Our serial experimental and in silico findings highlight the therapeutic potential of PIP NPs for FXTAS treatment.

Funding

This work was supported by the General Research Fund from the University Grant Council of Hong Kong SAR [Reference number: 14114221].

Conflicts of Interest

The authors declare no conflicts of interest.

Data Availability Statement

The data that support the findings of this study are available from the corresponding author upon reasonable request.

References

1. M. A. Leehey, "Fragile X-Associated Tremor/Ataxia Syndrome: Clinical Phenotype, Diagnosis, and Treatment," *Journal of Investigative Medicine* 57 (2009): 830–836, https://doi.org/10.2310/JIM.0b013e3181af59c4.

2. R. J. Hagerman, D. A. Hall, S. Coffey, et al., "Treatment of Fragile X-Associated Tremor Ataxia Syndrome (FXTAS) and Related Neurological Problems," *Clinical Interventions in Aging* 3 (2008): 251–262, https://doi.org/10.2147/cia.s1794.

3. A. M. Cabal-Herrera, N. Tassanakijpanich, M. J. Salcedo-Arellano, and R. J. Hagerman, "Fragile X-Associated Tremor/Ataxia Syndrome (FXTAS): Pathophysiology and Clinical Implications," *International Journal of Molecular Sciences* 21 (2020): 4391, https://doi.org/10.3390/ijms21124391.

4. M. Derbis, E. Kul, D. Niewiadomska, et al., "Short Antisense Oligonucleotides Alleviate the Pleiotropic Toxicity of RNA Harboring Expanded CGG Repeats," *Nature Communications* 12 (2021): 1265, https://doi.org/10.1038/s41467-021-21021-w.

5. D. A. Hall, E. Berry-Kravis, R. J. Hagerman, P. J. Hagerman, C. D. Rice, and M. A. Leehey, "Symptomatic Treatment in the Fragile X-Associated Tremor/Ataxia Syndrome," *Movement Disorders* 21 (2006): 1741–1744, https://doi.org/10.1002/mds.21001.

6. M. D. Disney, B. Liu, W.-Y. Yang, et al., "A Small Molecule that Targets r(CGG) Exp and Improves Defects in Fragile X-Associated Tremor Ataxia Syndrome," *ACS Chemical Biology* 7 (2012): 1711–1718, https://doi.org/10.1021/cb300135h.

7. M. Hagihara, H. He, M. Kimura, and K. Nakatani, "A Small Molecule Regulates Hairpin Structures in d(CGG) Trinucleotide Repeats," *Bioorganic & Medicinal Chemistry Letters* 22 (2012): 2000–2003, https://doi.org/10.1016/j.bmcl.2012.01.030.

8. A. Qurashi, H. Liu, L. Ray, D. L. Nelson, R. Duan, and P. Jin, "Chemical Screen Reveals Small Molecules Suppressing Fragile X Premutation rCGG Repeat-Mediated Neurodegeneration in Drosophila," *Human Molecular Genetics* 21 (2012): 2068–2075, https://doi.org/10.1093/hmg/dds024.

9. T. Tran, J. L. Childs-Disney, B. Liu, L. Guan, S. Rzuczek, and M. D. Disney, "Targeting the r(CGG) Repeats That Cause FXTAS With Modularly Assembled Small Molecules and Oligonucleotides," *ACS Chemical Biology* 9 (2014): 904–912, https://doi.org/10.1021/cb400875u.

10. A. K. Verma, E. Khan, S. K. Mishra, A. Mishra, N. Charlet-Berguerand, and A. Kumar, "Curcumin Regulates the r(CGG) Exp RNA Hairpin Structure and Ameliorate Defects in Fragile X-Associated Tremor Ataxia Syndrome," *Frontiers in Neuroscience* 14 (2020): 295, https://doi.org/10.3389/fnins.2020.00295.

11. A. K. Verma, E. Khan, S. K. Mishra, and A. Kumar, "Small Molecule Screening Discovers Compounds That Reduce FMRpolyG Protein Aggregates and Splicing Defect Toxicity in Fragile X-Associated Tremor/Ataxia Syndrome," *Molecular Neurobiology* 59 (2022): 1992–2007, https://doi.org/10.1007/s12035-021-02697-z.

12. A. K. Verma, E. Khan, S. K. Mishra, N. Jain, and A. Kumar, "Piperine Modulates Protein Mediated Toxicity in Fragile X-Associated Tremor/Ataxia Syndrome Through Interacting Expanded CGG Repeat (r(CGG) Exp) RNA," *ACS Chemical Neuroscience* 10 (2019): 3778–3788, https://doi.org/10.1021/acschemneuro.9b00282.

13. M. Boivin, R. Willemsen, R. K. Hukema, and C. Sellier, "Potential Pathogenic Mechanisms Underlying Fragile X Tremor Ataxia Syndrome: RAN Translation and/or RNA Gain-of-Function?," *European Journal of Medical Genetics* 61 (2018): 674–679, https://doi.org/10.1016/j.ejmg.2017.11.001.

14. T. Ren and Z. Zuo, "Role of Piperine in CNS Diseases: Pharmacodynamics, Pharmacokinetics and Drug Interactions," *Expert Opinion on Drug Metabolism & Toxicology* 15 (2019): 849–867, https://doi.org/10.1080/17425255.2019.1672658.

15. M. J. O'Neil, The Merck Index: An Encyclopedia of Chemicals, Drugs, and Biologicals (RSC Publishing, 2013).

16. J. Li, S. S. Y. Leung, E. H. Y. Chan, C. Jiang, E. T. Y. Ho, and Z. Zuo, "Significantly Increased Aqueous Solubility of Piperine via Nanoparticle Formulation Serves as the Most Critical Factor for Its Brain Uptake Enhancement," *International Journal of Nanomedicine* 20 (2025): 3945–3959, https://doi.org/10.2147/IJN.S506827.

17. H. E. Kong, J. Zhao, S. Xu, P. Jin, and Y. Jin, "Fragile X-Associated Tremor/Ataxia Syndrome: From Molecular Pathogenesis to Development of Therapeutics," *Frontiers in Cellular Neuroscience* 11 (2017): 128, https://doi.org/10.3389/fncel.2017.00128.

18. P. Jin, D. C. Zarnescu, F. Zhang, et al., "RNA-Mediated Neurodegeneration Caused by the Fragile X Premutation rCGG Repeats in Drosophila," *Neuron* 39 (2003): 739–747, https://doi.org/10.1016/s0896-6273(03)00533-6.

19. A. E. Linsalata, F. He, A. M. Malik, et al., "DDX 3X and Specific Initiation Factors Modulate FMR 1 Repeat-Associated Non-AUG-Initiated Translation," *EMBO Reports* 20 (2019): e47498–https://doi.org/10.15252/embr.201847498.

20. D. Van Dam, V. Errijgers, R. F. Kooy, et al., "Cognitive Decline, Neuromotor and Behavioural Disturbances in a Mouse Model for Fragile-X-associated Tremor/Ataxia Syndrome (FXTAS)," *Behavioural Brain Research* 162 (2005): 233–239, https://doi.org/10.1016/j.bbr.2005.03.007.

21. R. Willemsen, M. Hoogeveen-Westerveld, S. Reis, et al., "The FMR1 CGG Repeat Mouse Displays Ubiquitin-Positive Intranuclear Neuronal Inclusions; Implications for the Cerebellar Tremor/Ataxia Syndrome," *Human Molecular Genetics* 12 (2003): 949–959, https://doi.org/10.1093/hmg/ddg114.

22. R. M. Paim, M. H. Pereira, R. Di Ponzio, et al., "Validation of Reference Genes for Expression Analysis in the Salivary Gland and the Intestine of Rhodnius prolixus (Hemiptera, Reduviidae) Under Different Experimental Conditions by Quantitative Real-Time PCR," *BMC Research Notes* 5 (2012): 1–11, https://doi.org/10.1186/1756-0500-5-128.

23. Y. Kim, Y. Kim, and Y. H. Kim, "Evaluation of Reference Genes for Gene Expression Studies Using Quantitative Real-Time PCR in Drosophila melanogaster After Chemical Exposures," *Journal of Asia-Pacific Entomology* 23 (2020): 385–394, https://doi.org/10.1016/j.aspen.2020.01.008.

24. U. Schmidt, M. Weigert, C. Broaddus, and G. Myers, "Cell Detection With Star-convex Polygons," in International Conference on Medical Image Computing and Computer-Assisted Intervention (Springer, 2018), 265–273.

25. N.R. Council, Guide for the Care and Use of Laboratory Animals: Eighth Edition (National Academies Press, 2011).

26. M. I. Simon, Constitutive Activity in Receptors and Other Proteins, Part A (Academic Press, 2010).

27. C. González-Cabrera, K. Draggendorf, and M. Prigge, "Rotarod-Test for Mice," protocols.io (2024), https://doi.org/10.17504/protocols.io.14egn3qpml5d/v1.

28. S. Asamitsu, Y. Yabuki, S. Ikenoshita, et al., "CGG Repeat RNA G-Quadruplexes Interact With FMRpolyG to Cause Neuronal Dysfunction in Fragile X-Related Tremor/Ataxia Syndrome," *Science Advances* 7 (2021): eabd9440, https://doi.org/10.1126/sciadv.abd9440.

29. K. Chapman, F. Sewell, L. Allais, et al., "A Global Pharmaceutical Company Initiative: An Evidence-Based Approach to Define the Upper Limit of Body Weight Loss in Short Term Toxicity Studies," *Regulatory Toxicology and Pharmacology* 67 (2013): 27–38, https://doi.org/10.1016/j.yrtph.2013.04.003.

30. M. F. Balaha, A. A. Alamer, M. S. Abdel-Kader, and K. M. Alharthy, "Ameliorative Potential of (-) Pseudosemiglabrin in Mice With Pilocarpine-Induced Epilepsy: Antioxidant, Anti-Inflammatory, Anti-Apoptotic, and Neurotransmission Modulation," *International Journal of Molecular Sciences* 24 (2023): 10773, https://doi.org/10.3390/ijms241310773.

31. P. Chakraborty and F. Grosse, "Human DHX9 Helicase Preferentially Unwinds RNA-Containing Displacement Loops (R-Loops) and G-Quadruplexes," *DNA Repair* 10 (2011): 654–665, https://doi.org/10.1016/j.dnarep.2011.04.013.

32. P. Chakraborty, J. T. J. Huang, and K. Hiom, "DHX9 Helicase Promotes R-Loop Formation in Cells With Impaired RNA Splicing," *Nature Communications* 9 (2018): 4346, https://doi.org/10.1038/s41467-018-06677-1.

33. I. Malik, Y. J. Tseng, C. M. Wieland, et al., "Dissecting the Roles of EIF4G Homologs Reveals DAP5 as a Modifier of CGG Repeat-Associated Toxicity in a Drosophila Model of FXTAS," *Neurobiology of Disease* 184 (2023): 106212, https://doi.org/10.1016/j.nbd.2023.106212.

34. R. Rosenzweig, N. B. Nillegoda, M. P. Mayer, and B. Bukau, "The Hsp70 Chaperone Network," *Nature Reviews Molecular Cell Biology* 20 (2019): 665–680, https://doi.org/10.1038/s41580-019-0133-3.

35. G. Zazeri, A. P. R. Povinelli, M. F. Lima, and M. L. Cornélio, "Detailed Characterization of the Cooperative Binding of Piperine With Heat Shock Protein 70 by Molecular Biophysical Approaches," *Biomedicines* 8 (2020): 629, https://doi.org/10.3390/biomedicines8120629.

36. O. Trott and A. J. Olson, "AutoDock Vina: Improving the Speed and Accuracy of Docking With a New Scoring Function, Efficient Optimization, and Multithreading," *Journal of Computational Chemistry* 31 (2010): 455–461, https://doi.org/10.1002/jcc.21334.

37. H. J. Wenzel, M. R. Hunsaker, C. M. Greco, R. Willemsen, and R. F. Berman, "Ubiquitin-Positive Intranuclear Inclusions in Neuronal and Glial Cells in a Mouse Model of the Fragile X Premutation," *Brain Research* 1318 (2010): 155–166, https://doi.org/10.1016/j.brainres.2009.12.077.

38. M. R. Glineburg, P. K. Todd, N. Charlet-Berguerand, and C. Sellier, "Repeat-Associated Non-AUG (RAN) Translation and Other Molecular Mechanisms in Fragile X Tremor Ataxia Syndrome," *Brain Research* 1693 (2018): 43–54, https://doi.org/10.1016/j.brainres.2018.02.006.

39. I. P. Nezis, A. Simonsen, A. P. Sagona, et al., "Ref (2) P, the *Drosophila melanogaster* Homologue of Mammalian p62, Is Required for the Formation of Protein Aggregates in Adult Brain," *Journal of Cell Biology* 180 (2008): 1065–1071, https://doi.org/10.1083/jcb.200711108.

40. B. J. Bartlett, P. Isakson, J. Lewerenz, et al., "p62, Ref (2) P and Ubiquitinated Proteins Are Conserved Markers of Neuronal Aging, Aggregate Formation and Progressive Autophagic Defects," *Autophagy* 7 (2014): 572–583, https://doi.org/10.4161/auto.7.6.14943.

41. E. P. Ratliff, R. E. Mauntz, R. W. Kotzebue, et al., "Aging and Autophagic Function Influences the Progressive Decline of Adult

Drosophila Behaviors," *PLOS ONE* 10 (2015): e0132768, https://doi.org/10.1371/journal.pone.0132768.

42. Z. Ahmed, H. Sheng, Y.-f. Xu, et al., "Accelerated Lipofuscinosis and Ubiquitination in Granulin Knockout Mice Suggest a Role for Progranulin in Successful Aging," *American Journal of Pathology* 177 (2010): 311–324, https://doi.org/10.2353/ajpath.2010.090915.

43. A. Shimada, H. Keino, N. Kawamura, Y. Chiba, and M. Hosokawa, "Limbic Structures Are Prone to Age-Related Impairments in Proteasome Activity and Neuronal Ubiquitinated Inclusions in SAMP10 Mouse: A Model of Cerebral Degeneration," *Neuropathology and Applied Neurobiology* 34 (2008): 33–51, https://doi.org/10.1111/j.1365-2990.2007.00878.x.

44. L. Yang, Z. Ma, H. Wang, et al., "Ubiquitylome Study Identifies Increased Histone 2A Ubiquitylation as an Evolutionarily Conserved Aging Biomarker," *Nature Communications* 10 (2019), https://doi.org/10.1038/s41467-019-10136-w.

45. D. Dickson, A. Wertkin, Y. Kress, H. Ksiezak-Reding, and S. Yen, "Ubiquitin Immunoreactive Structures in Normal Human Brains," *Journal of Technical Methods and Pathology* 63 (1990): 87–99.

46. F. Mascadri, R. Ciccimarra, M. M. Bolognesi, F. Stellari, F. Ravanetti, and G. Cattoretti, "Background-Free Detection of Mouse Antibodies on Mouse Tissue by Anti-Isotype Secondary Antibodies," *Journal of Histochemistry & Cytochemistry* 69 (2021): 535–541, https://doi.org/10.1369/00221554211033239.

47. E. W. Schluter, M. R. Hunsaker, C. M. Greco, R. Willemsen, and R. F. Berman, "Distribution and Frequency of Intranuclear Inclusions in Female CGG KI Mice Modeling the Fragile X Premutation," *Brain Research* 1472 (2012): 124–137, https://doi.org/10.1016/j.brainres.2012.06.052.

48. T. Ren, Q. Wang, C. Li, M. Yang, and Z. Zuo, "Efficient Brain Uptake of Piperine and Its Pharmacokinetics Characterization After Oral Administration," *Xenobiotica* 48 (2018): 1249–1257, https://doi.org/10.1080/00498254.2017.1405293.

49. M. Drozd, S. Delhaye, T. Maurin, et al., "Reduction of Fmr1 mRNA Levels Rescues Pathological Features in Cortical Neurons in a Model of FXTAS," *Molecular Therapy Nucleic Acids* 18 (2019): 546–553, https://doi.org/10.1016/j.omtn.2019.09.018.

50. P. K. Todd, S. Y. Oh, A. Krans, et al., "CGG Repeat-Associated Translation Mediates Neurodegeneration in Fragile X Tremor Ataxia Syndrome," *Neuron* 78 (2013): 440–455, https://doi.org/10.1016/j.neuron.2013.03.026.

51. A. Tawani, A. Amanullah, A. Mishra, and A. Kumar, "Evidences for Piperine Inhibiting Cancer by Targeting Human G-Quadruplex DNA Sequences," *Scientific Reports* 6 (2016): 39239, https://doi.org/10.1038/srep39239.

52. N. Liberman, V. Gandin, Y. V. Svitkin, et al., "DAP5 Associates With eIF2β and eIF4AI to Promote Internal Ribosome Entry Site Driven Translation," *Nucleic Acids Research* 43 (2015): 3764–3775, https://doi.org/10.1093/nar/gkv205.

53. X. Lai, G. Pan, X. Feng, et al., "Targeting DAP5 Disrupts Alternate Mode of Translational Initiation in Tregs and Potentiates Antitumor Immunity," *Advanced Science* 13 (2026): e20625, https://doi.org/10.1002/advs.202520625.

54. X. Li, H. Shao, I. R. Taylor, and J. E. Gestwicki, "Targeting Allosteric Control Mechanisms in Heat Shock Protein 70 (Hsp70)," *Current Topics in Medicinal Chemistry* 16 (2016): 2729–2740, https://doi.org/10.2174/1568026616666160413140911.

55. A. M. Wang, Y. Miyata, S. Klinedinst, et al., "Activation of Hsp70 Reduces Neurotoxicity by Promoting Polyglutamine Protein Degradation," *Nature Chemical Biology* 9 (2013): 112–118, https://doi.org/10.1038/nchembio.1140.

Supporting Information

Additional supporting information can be found online in the Supporting Information section.